Reviews in Mineralogy & Geochemistry
Vol. 63, pp. 427-458, 2006

16

Internal Stresses in Deformed Crystalline Aggregates

Mark R. Daymond

Department of Materials Science and Engineering
Queens University
Kingston, Ontario, K7L 3N6, Canada
e-mail: daymond@me.queensu.ca

INTRODUCTION

This Chapter is an introduction to the various length scales of internal stresses, the causes of internal stresses and in particular their measurement by neutron diffraction. Some of the approaches used to model and interpret internal stresses are also introduced, and the use of these approaches to interpret deformation mechanisms illustrated through a number of examples.

In nearly every case when an engineering material is employed it will experience some stresses, if only those due to its own weight. Real materials are not the uniform continuum they are sometimes considered to be, and local differences in structure or properties mean that the local 'internal' stress is not necessarily equal to any external applied stress. These internal stresses are fundamental in controlling the deformation and failure of materials; they can have a considerable effect on material properties, including fatigue resistance, fracture toughness and strength. These stresses can vary greatly as a function of position within a body, due to the processes experienced during its production. Consequently, their measurement and interpretation is of considerable interest (e.g., Hutchings 1990), and great efforts have been employed over the years in developing accurate and precise measurement techniques. Such stresses can develop in a deformed material at many length scales and from many mechanisms. Fundamentally, internal stresses arise due to the elastic response of the material when an inhomogeneous distribution of non-elastic strains is imposed. These non-elastic strains could be due to plastic strain, precipitation, phase transformations, thermal expansion, etc. (Noyan and Cohen 1987). The origins in all cases thus come down simply to two aspects: heterogeneity and constraint. That is, when the various constituent parts of a component or material would, if unconstrained, exhibit different responses to the applied load (be that stress, temperature, electric field, etc.) the constraints imposed by the bulk of the surrounding material result in the build up of stresses between these constituent parts.

However, before the occurrence and impact of stresses in materials is discussed in some detail, the use of diffraction techniques for the measurement of stress is summarized, with an emphasis on neutron diffraction. Examples of the work carried out in the modeling of internal stresses will be reviewed in some detail, since it is the combination of experimental data with micromechanical modeling that has proven to be a highly fruitful area of research, providing great insight into the microscale deformation mechanisms which may be occurring. Considerable work has been carried out in this field in the study of the deformation of metals, and to a lesser extent in ceramics, and so it is here that the focus of the Chapter lies. However the Chapter also covers recent work applying these ideas to geological materials, and considers some of the particular issues which need to be addressed in applying the large body of work on engineering materials to geological systems.

1529-6466/06/0063-0016$05.00 DOI: 10.2138/rmg.2006.63.16

MEASUREMENT OF STRESS BY DIFFRACTION

One highly successful technique for making non-destructive measurements of stresses within engineering samples is diffraction, using either X-rays or other probes (Noyan and Cohen 1987). Conventional X-rays are limited to surface studies, while more penetrating radiation such as neutrons or synchrotron X-rays allow studies at greater depth in the material (Fitzpatrick and Lodini 2003). This has the attraction of allowing the study of bulk average properties, without the complications of the changing stress states and constraints which occur near the surface of a material. Many text books are available on the subject of the measurement of stresses by diffraction; while the aspects relevant to the study of deformation are summarized here, for more detailed and complete discussions the reader is referred either to the two books cited above or to, for example, Hauk (1997), Krawitz (2001) or Hutchings et al. (2005).

Length scales of stress

Those working in the measurement and interpretation of stresses typically classify the measured stresses according to the length scales over which they operate, relative to the microstructural repeat unit. The advent of new strain measurement techniques using EBSD (Wilkinson 1997) or synchrotron X-ray micro-diffraction (e.g., Martins et al. 2004) which probe materials at very short length scales are acting to blur these divisions somewhat, but the distinctions remain very useful. Macroscale or Type I stresses act over length scales at which the material can be considered to be a continuum, usually millimeters or larger. For example, the plastic deformation induced in the surface layers of a material by grinding or shot peening results in stresses in these layers because of the constraining effect of the bulk material below (Fig. 1); these stresses act over hundreds of micrometers. Other examples include the stresses in anything from bent bars and welded sheet metal, to the stresses between tectonic plates. Type I stresses are the stresses that would be of primary concern to a design engineer. A whole host of techniques, both destructive and non-destructive, are available for the measurement of such stresses, and a flavor of some of them can be found in the review by Ruud (1982). At the other

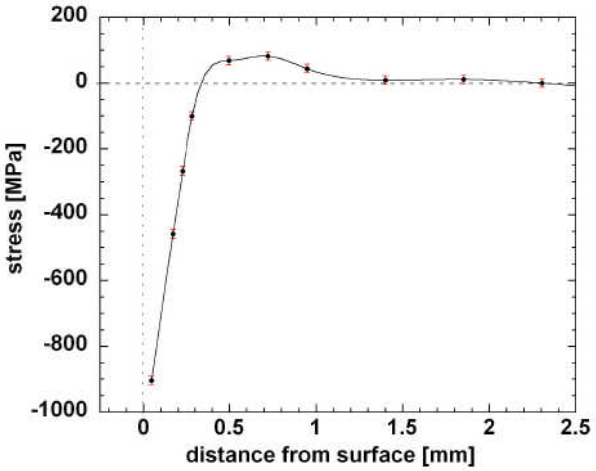

Figure 1. The stress profile generated by shot peening of a nickel plate, illustrating the Type I stress component in the direction in the plane of the surface of the plate. Plasticity is expected to have occurred in approximately the top 0.25 mm of material and generates compressive stresses near the surface with balancing tensile stresses deeper in the material. Data was obtained by the author on the ENGIN instrument at the ISIS pulsed neutron source, as part of the VAMAS TWA20 exercise (Webster 2001), and is previously unpublished. Lines are a guide to the eye.

end of the lengthscale, Type III stresses vary *within* the individual length scale of the microstructure, i.e., within the grain or crystallite. They may vary on the level of the atomic lattice arising from, for example, atomic vacancies, the distortion of the lattice caused by dislocations, or the strains at a semi-coherent precipitate interface. In contrast, Type II stresses vary on the intermediate length scale which is comparable to that of the microstructure repeat unit. For example, the different properties of the phases of a composite lead to so-called "interphase" Type II stresses (see below).

Figure 2 is a schematic illustrating the different length scales of stress discussed above, and how they relate to a microstructure. The stresses experienced at any given position in the material will be a summation of the various types described above. The discussion in this Chapter will consider mainly Type II stresses, with a more cursory treatment of Type I and III, because it is Type II stresses which are principally important in interpreting and understanding the response of the polycrystalline aggregate to applied load. However the various techniques for the measurement of internal stresses will be sensitive to the different types in different ways, and so some attention is given to the other types as necessary. In the literature a distinction is usually drawn between residual and internal stresses; the former are those which are self-equilibrating in a body which has no external forces or constraints acting on it. They will be additive to those stresses arising from any applied load; the internal stresses are thus a combination of the residual and those due to the applied stresses.

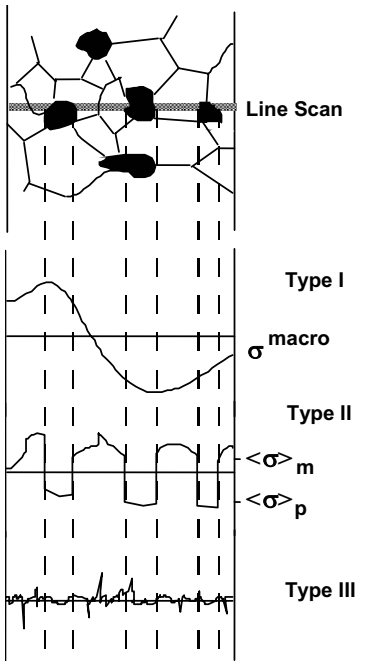

Figure 2. Schematic illustrating the length scales of stresses. The top part of the figure illustrates a microstructure, with different grains, and different phases (light/dark). The stresses that exist along the line scan shown are indicated in the lower part of the figure. Type I stress vary on a long length scale, while Type II stresses vary on the scale of the microstructure, as a function of phase (e.g. matrix $\langle\sigma\rangle_m$ and particle $\langle\sigma\rangle_p$, where "<>" indicates "average") as well as a function of grain orientation within the phase. Type III stresses vary within the microstructural element. The total stress at any given position in the material is the sum of the three stress contributions. [Reprinted from Fitzpatrick et al. (1997), Fig. 1, with permission of Elsevier].

Experimental arrangements

Neutron diffraction can be used to measure components of the strain tensor directly from changes in crystal lattice spacing. When illuminated by radiation of wavelength similar to atomic lattice spacings, crystalline materials diffract this radiation as distinctive Bragg peaks. The stress experienced by the material causes a change in the spacing of the atomic lattice. If the entire volume that is diffracting and contributing to a particular diffraction peak has a change in mean elastic strain, that diffraction peak moves. This is the case for Type I and Type II stresses. In contrast, if the average stress in the diffracting volume remains constant but the *distribution* of stresses changes, the shape and width of the peak changes. This effect on diffraction peaks is caused by Type III stresses, and by changes in the distribution of Type II stresses.

Determination of strain

The two classes of sources of neutron source, monochromatic and time-of-flight, can both be used for the measurement of strain. For a monochromatic wavelength source, differentiation of Bragg's law gives:

$$\varepsilon = \left(\frac{\Delta d}{d_0} \right) = -\Delta\theta \cot\theta_0 \tag{1}$$

where $\Delta\theta$ is in radians, and the values θ_0 and d_0 are those obtained in a stress-free sample of the material. Type I and Type II stresses both cause a change in position of the diffraction peak—it is this change which is measured and interpreted as strain, based on Equation (1). Type III stresses, on the other hand, cause a change in the width of the diffraction peak; their analysis is outside the scope of this review, but see e.g. (Warren 1990; Gubicza et al. 2004; Mittemeijer and Scardi 2004). To be confident of correctly determining the peak position, it is important that an appropriate peak shape is used in the peak fitting process, particularly in the case where changes in width may occur. As discussed elsewhere in this issue (Vogel and Priesmeyer 2006, this volume), typically Gaussian or pseudo-Voigt peak shapes are used (e.g., Hutchings et al. 2005).

The neutron diffraction instruments that are used for strain measurements are, in their principles of operation, very similar to general purpose powder diffraction instruments. A number of key differences exist however. Firstly, in contrast to conventional powder diffraction, but in the same way as for texture measurements, when measuring elastic strains it is important to note that the direction in which the strains are measured relative to the sample becomes a critical aspect of the data analysis. The direction in which strain is measured is along the scattering vector **Q**, which is perpendicular to the diffracting planes shown as diagonal lines in Figure 3a. When measuring multiple diffraction peaks (each with different θ_0) in a particular direction in the sample, the sample/detector configuration is usually reoriented such that the scattering vector **Q** always lies in the same orientation relative to the sample. It should be noted that, in general, for each *hkl* diffraction peak a different strain will be determined, due to both differences in the elastic stiffnesses and to plastic anisotropy, as will be discussed below in the sections on intergranular strains. Secondly, such instruments are often used to make measurements to determine the internal stress occurring in large engineering components, or on samples contained within bulky sample environment facilities (required to impose temperature, stress etc. on the samples). As such there are certain physical constraints on the diffraction instrument, particularly the requirement of accurate physical positioning (typically ±0.05 mm) of large objects relative to the diffraction beam. The concepts involved behind the design of a neutron diffraction instrument are discussed in detail by Johnson and Daymond (2002).

At a time-of-flight (TOF) neutron scattering instrument, neutron pulses, each with a continuous range of velocities and therefore wavelengths, are directed at a specimen. The incident spectra are polychromatic, thus many lattice planes are recorded in each measurement. The scattering vectors **Q** for all reflections recorded in a given detector lie in the same direction, and thus measure the strain in that same direction. It should be emphasized again that each reflection is produced from a particular family of grains that are oriented such that a specific *hkl* plane diffracts to the detector. Strain can then be calculated from the shift in a given reflection:

$$\varepsilon_{hkl} = \frac{\Delta t}{t_0} = \frac{\Delta d}{d_0} = \frac{\Delta\lambda}{\lambda_0} \tag{2}$$

Figure 3 (*on facing page*). (a) Schematic illustrating the experimental arrangement for measurement of strains at a monochromatic neutron source. The strain is measured in the direction "Q" (e.g., Webster 2001). The diagonal hash lines indicate the measurement volume, and the orientation of the lattice planes which are diffracting. (b) Schematic illustrating the experimental arrangement for measurement of strains at a time-of-flight neutron source. The strain is measured simultaneously in the two directions "Q" (e.g., Webster 2001). The cross hash lines indicate the measurement volume, and the orientation of the two sets of lattice planes which are diffracting. (c) Schematic of the Engin-X beamline for strain measurement at ISIS. Components are: a) incident beam definition (guide and slits); b) neutron detectors; c) positioning table (x-y-z-θ); d) scattered beam definition (radial collimator); e) sample (sphere).

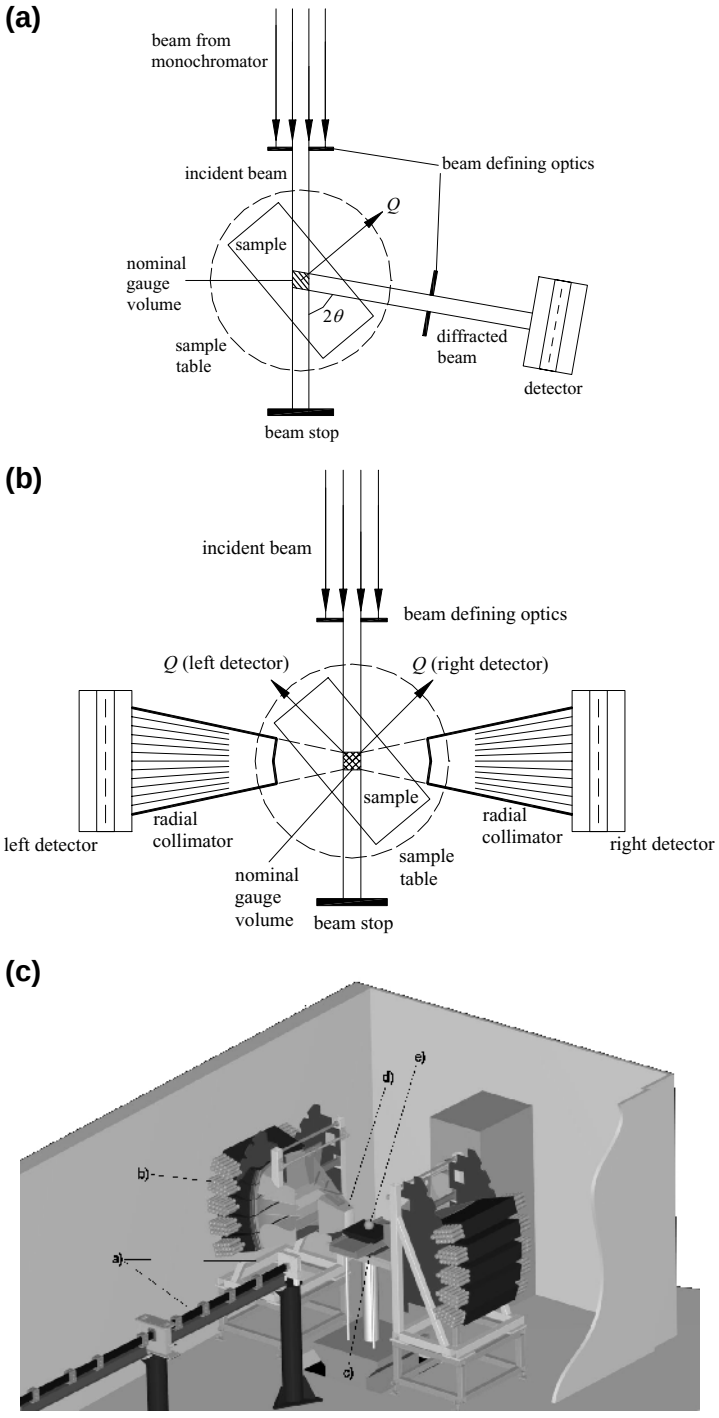

Figure 3. *caption on facing page*

where t is the time-of-flight, d is the lattice spacing and λ is the wavelength. However, since an entire diffraction spectrum with multiple diffraction peaks is obtained for each measurement direction, without the need for any reorientation of sample or detector, it is common practice in the measurement of Type I strains/stresses that instead of analyzing individual diffraction peaks, the strain is determined from the whole diffraction pattern using a Rietveld (1969) style analysis where a model of the crystallographic structure is used to create a simultaneous fit to the entire diffraction spectrum. In this case, strain is given by:

$$\varepsilon = \frac{\Delta a}{a_0} \tag{3}$$

where Δa is the change in lattice parameter relative to the lattice parameter a_0 of a stress-free or reference sample of the material. The strain determined by changes in the lattice parameter in this way from a conventional Rietveld refinement will be only slightly and subtly affected by any Type II stresses, hence its common use for the determination of Type I stresses. The impact of Type II stresses on Rietveld refinements and ways in which the effects can be incorporated and utilized are described by Daymond et al. (1997, 1999a). The diffraction peak observed at TOF sources has a distinct asymmetry, due to the way that the neutrons are produced. However this asymmetry can be easily characterized as an instrumental parameter, and thus an appropriate peak shape used in the fitting procedure (e.g., Ikeda and Carpenter 1985).

The uncertainty in strain u_ε is given by (e.g., Webster 2001):

$$u_\varepsilon^2 = \frac{u_d^2}{d^2} + \frac{u_{d_0}^2}{d_0^2} \tag{4}$$

where

$$u_d^2 = d^2\left[\frac{u_\lambda^2}{\lambda^2} + u_\theta^2 \cot^2\theta\right] \tag{5}$$

Equation (4) is the correct value of the overall uncertainty for the strain. However if the same value of d_0 is used to calculate a series of strain measurements, their *relative* uncertainties are more simply given by:

$$u_\varepsilon^2 = \frac{u_d^2}{d^2} \tag{6}$$

The impact of background and the instrument resolution on the strain accuracy obtained, and thus subsequently on the count times required for a given measurement is discussed by Withers et al. (2001).

Some readers may be familiar with the $\sin^2\psi$ technique used in the measurement of stress by the diffraction of conventional X-rays (e.g., Noyan and Cohen 1987; Hauk 1997). Exactly the same methodology may be employed in neutron diffraction (Hauk 1997), however the imperative for it with conventional X-rays—namely that the small penetration depth means that strains can only be measured in reflection and not in transmission—is not present for neutrons. The technique is thus only sometimes used, since although it adds information and accuracy, it requires more experimental time.

By suitable use of slits and focusing mechanisms on both the incident and scattered beam, neutron diffraction can be used to determine the elastic strain *within a defined volume* in a polycrystalline solid (shown as diagonal hash shading in Fig. 3a). By moving the sample relative to this volume (which is fixed by the geometry of the diffraction apparatus), it is possible to build up a map of the spatial variation of strain, and/or phases present. The minimum spatial resolution presently achievable by this technique with neutron diffraction is of the order of 1/3 or 1/2

mm, but experiments carried out with spatial resolutions of between 1 to 4 mm are more common. Careful spatial alignment of the beam-defining mechanisms and the sample are required when carrying out mapping of the variation of strains as a function of position in an object. This is now a common and well established technique for engineering components (e.g., Preuss et al. 2002; Edwards et al. 2005), and the technique has also been applied to the mapping of archaeological (Siano et al. 2006) and geological (Meredith et al. 1997; Scheffzük et al. 2005) samples. Some interesting work has looked at mapping the strains occurring around a crack tip under load (Sun et al. 2005), although the high spatial resolution required for this often makes such studies more suited to synchrotron X-rays (Withers et al. 2002), as discussed below. For a detailed description of the experimental methods and potential pitfalls involved in making spatial mapping measurements, which is outside the scope of this review, the reader should consult Webster (2001) or Hutchings et al. (2005).

Table 1. Neutron sources with dedicated strain measurement facilities.

Facility
AEC, South Africa
ANSTO, Australia
FRM-2, Germany
GKSS, Germany
HiFR, ORNL, USA
HMI, Germany
ILL, France
ISIS, UK
JAERI, Japan
JRC, Netherlands
KAERI, S. Korea
KUR, Japan
LANSCE, LANL, USA
LLB, France
MURR, USA
NIST, USA
NPI, Czech Republic
NRC, Canada
PSI, Switzerland
SNS, USA (under construction)

This section has introduced the key requirements of a neutron diffractometer used to measure stresses, which are similar for both monochromatic and time-of-flight neutron sources. These are a well defined incident beams which are critical to spatial mapping measurements; standard detectors appropriate for the type of source; a method to define where in the sample the scattered beam originates, which is dependent on the type of source; and a high capacity, high precision table capable of moving objects relative to the neutron beam. Typical capacities for such tables in modern instruments might be 500 kg, with 500 mm of travel, and 0.01 mm/100 mm precision. A schematic of one of the most recent stress measurement diffractometers, ENGIN-X (Santisteban et al. 2006a) is given in Figure 3c, and illustrates these components. A list of neutron sources which have neutron diffractometers dedicated to strain measurement is given in Table 1 (after Webster 2001). The GKSS, ISIS, LANSCE, SNS and PSI facilities have pulsed neutron strain measurement diffractometers, while the other facilities in Table 1 have monochromatic neutron strain measurement diffractometers. The benefit of the pulsed neutron sources for strain measurements is that, as already stated, a large number of diffraction peaks are easily obtained. The major benefit of the monochromatic sources is that if only one or a small number of diffraction peaks are required, data acquisition times are usually lower than at a pulsed source.

Calculation of stresses

So far we have considered only the measurement of strains. Stress and elastic strain are second rank tensors which are related through the elastic constants of a solid. Given the strain it is therefore possible to calculate the *stress* in the scattering volume provided the relevant material elastic constants are known. Determination of the full strain tensor requires measurements of the elastic strain along at least six independent directions. If the principal strain directions within the body are known this can be reduced, typically to three orthogonal directions. The conversion of strain to stress follows a slight modification of the well-known equations that are used for isotropic solid state mechanics (Hooke's law):

$$\sigma_{xx} = \frac{E_{hkl}}{(1+\nu_{hkl})(1-2\nu_{hkl})}\left[(1-\nu_{hkl})\varepsilon_{xx} + \nu_{hkl}\left(\varepsilon_{yy}+\varepsilon_{zz}\right)\right] \quad (7)$$

where E_{hkl} and ν_{hkl} represent the Young's modulus and Poisson's ratio respectively appropriate for the given *hkl* lattice reflection, and ε_{ii} and σ_{ii} represent the strain and stress respectively in the directions indicated. The choice of values for E_{hkl} and ν_{hkl} is discussed in more detail in the section on diffraction elastic constants. It should be noted that Equation (7) can be used even when the strains are not in principal directions, provided that they are orthogonal. However in this case, the stresses determined will also not necessarily be principal stresses, i.e., the presence of any shear stresses is ignored. Typically principal directions are assumed based on sample/experiment geometry, with the actual experimental determination of principal direction (Krawitz and Winholtz 1994) being the exception, rather than the rule.

In the case of the Rietveld analysis of multiple diffraction peaks, typically the macroscopic elastic properties would be the appropriate ones to be used in Equation (7), as justified empirically by Daymond et al. (1997, 1999a), and somewhat more rigorously in (Daymond 2004). Authors have also suggested alternate multi-peak averaging approaches appropriate for the study of Type I stresses (Kamminga et al. 2000; Daymond 2004).

Comparison with some other techniques

A range of other scattering techniques are available for the measurement of strain, most obviously conventional X-rays (e.g., Noyan and Cohen 1987), but also including high energy synchrotron X-rays (e.g., Fitzpatrick and Lodini 2003) and EBSD (Wilkinson 1997). A major difference in comparison with conventional X-ray or electron diffraction is that the path length of thermal neutrons is much higher for most materials. Thus, while conventional X-rays and electrons probe the surface layers of materials, neutrons interact with the "bulk" of the material. This has a particular impact when considering the stress state found in phases or grains. The near surface will be in plane stress conditions, since the stress component normal to a free surface must be zero. This is likely to be very different from the stress state found within the depth of a material, where the constraint of surrounding grains plays a significant role in the development of internal stresses.

High energy synchrotron X-rays can, however, have a path length which, while typically smaller is certainly close to that of neutrons, particularly for lighter elements (Table 2). With the growing availability of high energy synchrotron sources in the last 10 years, the engineering neutron diffraction strain measurement community has rapidly taken on board the new technique. The first synchrotron X-ray diffractometers which will be dedicated at least part time to strain measurement are presently under commissioning or construction. The great benefit of synchrotron X-rays over neutrons is that a very high flux is obtained, typically allowing 1s data acquisition times, which should be compared to around 100 s at neutron facilities under optimum conditions. Synchrotron X-rays have a very low divergence compared to neutrons. While this has the advantage that it is easy to produce a small beam size if such is desired, it has the negative consequence that for large (20 μm+) grain size samples (see below) very few

Table 2. Approximate attenuation lengths (63% reduction in intensity) for laboratory X-rays, synchrotron X-rays and neutrons. Adapted from (Withers 2004).

Source	Energy (keV)	Wavelength (Å)	Approximate attenuation length (mm)				
			Al	Ti	Fe	Ni	Cu
Thermal neutrons	2.5×10^{-5}	1.80	96	18	8	5	10
Synchrotron X-rays	150	0.08	39	14	7	5	5
Synchrotron X-rays	60	0.21	13	3	1.1	0.8	0.7
Synchrotron X-rays	31	0.40	3.3	1	0.16	0.11	0.10
Lab. X-rays (Cu Kα)	8.05	1.54	0.076	0.011	0.004	0.023	0.021

grains within the sample are at the diffraction condition, which may mean that the diffraction pattern obtained does not represent a "powder average." In such cases it may be possible to "rock" the sample during data acquisition to bring more grains into the diffraction condition, or alternately to take advantage of this fact and simply measure these single grains within the polycrystal and thus to interpret their behavior directly (e.g., Martins et al. 2004) rather than via a polycrystal average. At the high X-ray energies typically used for such measurements, the wavelength of the X-rays is very small, resulting in a smaller scattering angle than found with neutrons. For example, an 80 keV X-ray has a wavelength of ~0.15 Å. For a steel (111) diffraction peak, this results in a scattering angle $2\theta = 4°$, compared with a 2θ close to 90° for thermal neutrons. This difference in scattering geometry has an impact on many experimental considerations, and is discussed in more detail in (Fitzpatrick and Lodini 2003). One result is that the depth at which a strain can be measured in an object is highly dependent on which component of strain is being measured relative to the surfaces, meaning that in much of the published literature only in-plane components of strain are reported. While this has an impact on "strain scanning" measurements, it is often not an issue for *in situ* loading experiments and such measurements have become increasingly popular where sample constraints allow (e.g., Daymond and Withers 1996b; Pyzalla et al. 2006).

Finally, we mention in passing the technique of pulsed neutron transmission strain measurement. The transmission spectrum of thermal neutrons through a polycrystalline sample displays sudden, well-defined increases in intensity as a function of neutron wavelength. These Bragg edges occur because for a given *hkl* reflection, the Bragg angle increases as the wavelength increases until 2θ is equal to 180°. At wavelengths greater than this critical value, no scattering by this particular *hkl* lattice spacing can occur, and there is a sharp increase in the transmitted intensity. The transmitted spectrum can be analyzed (Santisteban et al. 2002) and changes in the position of these sharp changes in intensity interpreted as changes in the elastic strain, with the scattering vector $\mathbf{Q}$ being along the direction of the neutron beam. The set-up in such experiments is simple; the sample is placed in a collimated pulsed neutron beam, and the detector is located in line behind the sample. By using a two-dimensional array of detectors it is possible to map the lattice spacing in simple geometry samples, producing images analogous to neutron radiography although with to-date only millimeter resolution. The technique has been applied to archaeological samples (Siano et al. 2006), and single crystals (Santisteban et al. 2006b) as well as to engineering structures (Santisteban et al. 2002). However the technique requires a white beam of neutrons from a pulsed source and at present is only available at a small number of facilities; the ENGIN-X instrument at ISIS is equipped with a transmission detector which can operate simultaneously with the conventional diffraction detectors.

INTERNAL STRESSES

Some of the example studies described below detail measurements and studies of residual stresses, that is those present in a material due to its previous thermo-mechanical processing. A common origin of such residual stresses is due to thermal misfit, that is differing thermal contractions/expansions between different parts of the sample after exposure to elevated temperatures. However, many studies published have considered not just residual stresses, but the generation of stresses during *in situ* loading. In this way, the deformation history of a single sample can be monitored without the ambiguity of making measurements on a suite of pre-deformed samples. In this case, typically a conventional hydraulic or screw driven loading frame is used, oriented appropriately relative to the diffraction scattering geometry. The majority of work to date in this area has considered simple uniaxial loading. The applied load is usually incremented, and held at constant macroscopic stress (or strain) while neutron data are collected, before the load or strain is again incremented. Typically the load frame is oriented in the neutron diffractometer such that the scattering vector lies either on the axis parallel to the

loading direction or perpendicular to it, thus exploring the axial strains and the Poisson strains, i.e., parallel and perpendicular to the applied load respectively (see e.g., Fig. 3b). An example of such an apparatus and its use is described in detail by (Daymond and Priesmeyer 2002). Other additions to such *in situ* loading facilities might include simultaneous heating (Ma et al. 2005) or cooling (Oliver et al. 2004c) of the sample. More recent work has started to address the perceived requirement for loading under elevated confining pressures (Covey-Crump et al. 2006a).

The advantage of diffraction in the study of multiphase polycrystalline materials becomes clear. Since in such samples each crystalline phase will produce a different diffraction pattern, the lattice parameter (or individual peak position) for each phase can be determined and monitored during deformation. By monitoring the changes in the lattice parameter the relative strains (and hence stresses) in each phase can be determined, and compared with the bulk sample response. Thus during *in situ* loading, assuming that the individual phase elastic properties are known, the fraction of the applied load borne by each phase can be determined. The lattice strain is a purely elastic measure, whether the composite as a whole is deforming elastically or plastically. The plastic deformation is thus interpreted based on the nature of load transfer between phases (or grain orientations as will be discussed), and from changes in peak width. It should be noted that recent work (Poulsen et al. 2005) has suggested that even amorphous structures, with their very different scattering characteristics, are susceptible to some of the treatments described here, but this is very much "work in progress."

Interphase stresses

It is perhaps easiest to understand the origin of Type II internal stresses when we consider the deformation of a composite material. Man-made composites have become ubiquitous; materials that are produced by physical mixing and interpenetration of individual phases, designed to provide properties which are, overall, superior to those of the individual constituent phases. Man mimics nature in this case since most natural materials are in fact composites of some form. The understanding of the way that the properties of the individual phases combine to produce the properties of the composite, and the distribution and transfer of stress between the phases of a composite during deformation, has long been an area of interest due to the influence of these stresses on the properties of the bulk composite material. In a multiphase material, the stresses arising between the phases can be considered to be due to shape misfit between the phases and to have two general origins: load transfer arising from differences in the elastic properties of the two phases; and "shape misfits" caused by effects such as differential thermal expansion or differential plastic flow (e.g., Clyne and Withers 1993). Figure 4 shows a schematic illustrating the origin of interphase stresses due to thermal misfit strains.

During loading of a sample, differences in the elastic properties of the phases lead to internal stresses and the distribution of load between the phases. Subsequent plastic flow due to local differences in yield stress and hardening coefficient causes local reaction stresses and thus redistribution of the applied load. The various micromechanical effects often give multiphase materials improved properties relative to their constituent phase, but sometimes they may also be detrimental and therefore must be understood to allow the use of composites use in real components. Many neutron diffraction studies have demonstrated the load partitioning between phases occurring in multi-phase metal-based composite systems, typically in situations where one phase does not yield (e.g., Withers et al. 1989; Allen et al. 1992; Bourke et al. 1993; Withers and Clarke 1998), although a number of systems where both phases potentially exhibit plastic behavior have also been studied (e.g., Dunst and Mecking 1996; Carter and Bourke 2000).

Consider the data shown in Figure 5, which shows the elastic strains in a Cu-Mo composite under applied loading to a few percent plastic strains (Daymond et al. 1999b). The Mo constitutes 15 vol% of the composite as a whole and is made up of discrete approximately equiaxed particles in a continuous Cu matrix. As is common for such measurements the strains are shown relative to the starting unstressed value, that is the quoted strains are not

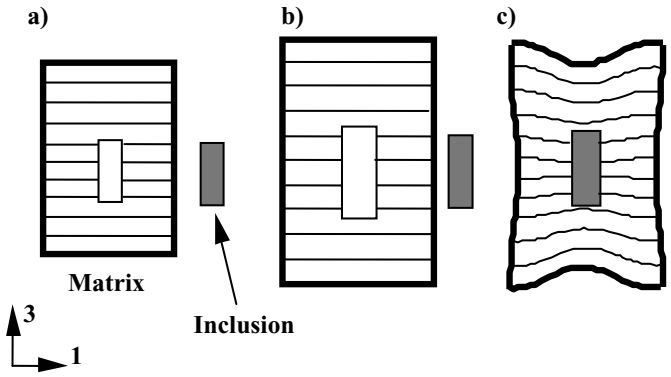

Figure 4. Schematic demonstrating the origin of thermal misfit strains, due to a rise in temperature on an idealized single reinforcement / matrix composite. Consider first an inclusion that fits exactly within a hole in the matrix. a) The inclusion is separated from the matrix. b) Both are heated, resulting in an expansion of the matrix and inclusion; the matrix expands more than the inclusion due to a higher coefficient of thermal expansion. c) The matrix and inclusion are joined back together; the reinforcement is in tension (pulled larger than it would otherwise be) and the matrix must have balancing compression.

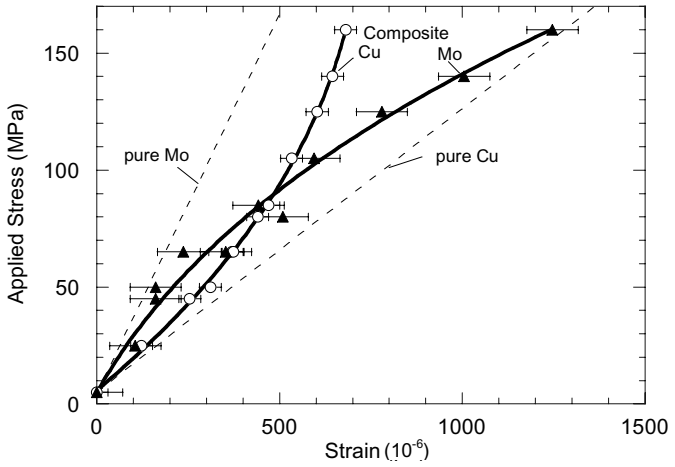

Figure 5. The internal phase strains measured by neutron diffraction in a Cu-Mo composite undergoing quasistatic tensile deformation. Lines are a guide to the eye. The nominal moduli for the pure phases is also shown (Used with permission. Fig. 3a from Daymond et al. 1999b).

absolute, since they do not take into account any initial thermal residual stresses produced during fabrication. The strains are the elastic strains parallel to the applied load as measured by diffraction. The experimental scatter shown (±30 με in the Cu and ±70 με in the Mo, where με represents a strain of 10^{-6}) was determined from the average error in lattice parameter calculated from the statistics of the diffraction analysis. The larger errors in the Mo phase are due to the smaller scattering volume and concomitant poorer counting statistics.

For applied stresses below 70 MPa, the reinforcement and matrix exhibit a linear response, with apparent moduli (slope of applied stress vs. elastic strain) which are within the limits imposed by the single phase Young's moduli. However, the strains in the Mo reinforcement are larger than in a hypothetical pure Mo sample and the strains in the Cu matrix are smaller than

a hypothetical pure Cu sample. From this we can infer that elastic load transfer occurs from the compliant Cu matrix to the stiffer Mo inclusions, demonstrating the effect of constraint simply in the elastic regime. At a stress of around 80 MPa, plasticity starts to occur in the Cu matrix, which has a lower yield stress than Mo. For a further given increment in applied stress the increase in elastic strain (i.e., stress) in the Cu is now smaller than in the elastic regime. Correspondingly, the increment in elastic strain in the plastically harder (non-yielding) Mo phase is larger than in the elastic regime. This is a classic demonstration of composite plastic load transfer (Clyne and Withers 1993).

Intergranular strains – elastic anisotropy

At a smaller length scale, we must take into account that for almost all materials the elastic stiffness of a single crystal (or crystallite) of material is dependent on its orientation relative to the applied load. This elastic anisotropy leads to a variation in the internal strains (and hence stresses) which are experienced by differently oriented grains in a polycrystal due to an applied load. The most well known result of this effect, is the requirement to use "diffraction elastic constants" or "plane specific stiffnesses" when making diffraction measurements of stress.

The elastic anisotropy of crystal structures in general is treated in many texts, for example, (Nye 1992). The treatment below summarizes that given by Nye, but considers only the high symmetry cubic and hexagonal structures. These make up the majority of engineering, though not geological materials. Using the conventional collapsed tensor notation (Nye 1992) of strain (ε), stress (σ), stiffness (C) and compliance (S) and the summation convention:

$$\varepsilon_i = S_{ik}\sigma_k \quad \text{and} \quad \sigma_i = C_{ik}\varepsilon_k \tag{8}$$

For a *single crystal* with cubic symmetry, it is found that

$$\frac{1}{E_{hkl}} = S_{11} - 2\left(S_{11} - S_{12} - \tfrac{1}{2}S_{44}\right)A_{hkl} \tag{9}$$

where E_{hkl} is the plane specific Young's modulus of the single crystal, and

$$A_{hkl} = \frac{\left(h^2k^2 + h^2l^2 + k^2l^2\right)}{\left(h^2 + k^2 + l^2\right)^2} \tag{10}$$

and thus has limiting values of $A_{h00} = 0$ and $A_{hhh} = {}^1/_3$. Hence the term $2(S_{11} - S_{12} - {}^1/_2 S_{44})$ governs the anisotropy of cubic materials, that is the way that the stiffness varies as a function of *hkl*. It is often reported as the dimensionless "cubic anisotropy factor" $2(S_{11} - S_{12})/S_{44} = 2C_{44}/(C_{11} - C_{12})$ with values in metals ranging from 0.71 in chromium, to 1.01 for the nearly isotropic tungsten, to 3.38 for copper (Hosford 1993). In the case of a *polycrystal*, the anisotropy inherent in the individual crystallite response given in Equation (9) will still be apparent. However, in the same way that the apparent moduli of the phases in the two phase composite described in the previous section were altered by the elastic load transfer and brought closer together than the individual phase moduli, the values of E_{hkl} in the polycrystal will not be as extreme as that seen in the single crystal. That is, while in copper we expect the plane specific modulus E_{200} of the *polycrystal* (determined by examining the response of the {200} type diffraction peak—the diffraction elastic constant) to be lower than that of E_{111}, in practice the difference between the two values will be smaller than that given by Equation (9) for a *single crystal*. The determination of the plane specific diffraction elastic constant of a polycrystal requires the use of the modeling approaches described in the next section. We note in passing however, that a linear variation with modulus as a function of A_{hkl} is still expected to hold for an untextured cubic polycrystal (Bollenrath et al. 1967), i.e., for a random polycrystal:

$$\frac{1}{E_{hkl}} = S - S'A_{hkl} \tag{11}$$

where S and S' are related to S_{11}, S_{12}, S_{44} via the polycrystal averaging method used (see section on models below). For the majority of cubic metals $E_{111} > E_{200}$ however there are some exceptions where the anisotropy is in the opposite sense such as chromium and niobium, and this is also the case for some inorganic phases, such as NaCl.

Due to the elastic anisotropy of the individual crystallites, the presence of texture has an influence on the observed elastic response of a polycrystalline aggregate. This is discussed in more detail in the section covering diffraction elastic constants.

For hexagonal structures, as would be expected given the lower symmetry, a more complicated expression holds and three parameters are required to describe the variation in elastic stiffness as a function of *hkl.* The variation is solely as a function of angle relative to the "*c*" axis, with the elastic stiffness being isotropic within the "*a*" plane. For hexagonal structures the appropriate expression is

$$\frac{1}{E_{hkl}} = \left(1 - L^2\right)^2 S_{11} + L^4 S_{33} + \left(1 - L^2\right) L^2 \left(2S_{13} + S_{44}\right) \tag{12}$$

where L is the cosine of the angle between the unit vector of the *hkl* plane normal and the hexagonal *c*-axis. As symmetry is reduced further, more and more parameters are required to describe the variation of elastic stiffness with crystallographic direction, for example see Nye (1992).

Intergranular strains – plastic anisotropy

As slip occurs preferentially on certain slip systems (plastic anisotropy), plastic relaxations lead to a further level of misfit stresses which is dependent on grain orientation. In effect one can consider the polycrystal as a composite in which every orientation of grain has a slightly different yield stress, thereby producing a highly complex stress-strain response. While long known of (Greenough 1947, 1952) these strains due to plastic anisotropy became of interest to the neutron diffraction community (MacEwen et al. 1983) more recently, in particular because of the potential to validate micromechanical plasticity models (see below). In Figure 6 the response of the lattice reflections with the five largest *d*-spacing are plotted against the applied stress for a single phase austenitic (*fcc*) stainless steel undergoing tensile loading (Daymond et al. 1997). Also shown is the 0.2% strain yield limit for plasticity, commonly used to determine the onset of macroscopic plasticity (e.g., Dieter 1986). It is worth re-iterating that each line represents the response of a family of grains within the polycrystal which are oriented such that the given *hkl* lattice plane is parallel to the loading direction. As expected, the initial response is elastic (linear), as described in the previous section. Deviations from linearity of the individual plane responses occur close to the onset of macroscopic plasticity. Once plastic deformation occurs, the yield of preferentially oriented grains relative to their neighbors causes strain redistribution, and there is a strong divergence from the hitherto linear response. In direct analogy to the description of the generation of interphase stresses in the section above, as subsets of grains become plastic, they do not accumulate elastic load at the same rate as they did when they where elastic, causing changes in the partitioning between the different grain orientations for a given incremental load increase. The first diffraction peaks that show evidence of the onset of plasticity in this case were the 531 (not shown) and 331 reflections, which showed an upward inflection at about 200 MPa (Clausen et al. 1999). These grain families thus play the part of plastically "soft" directions, with corresponding load transfer to the grains that are still deforming elastically, such as the 200 grains. However in contrast to the Cu-Mo example given above, at around 260 MPa this latter grain family also starts to

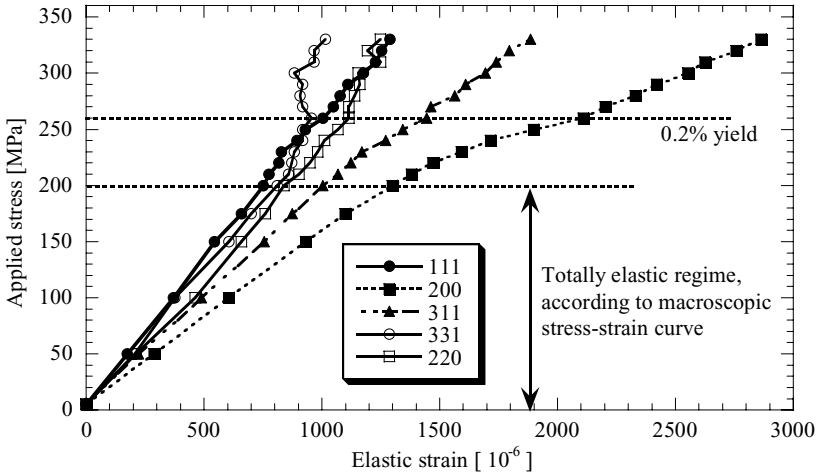

Figure 6. The internal strains measured on different diffraction peaks in a stainless steel undergoing quasistatic tensile deformation. Lines are a guide to the eye. (Used with permission of American Institute of Physics, Fig, 2 in Daymond et al. 1997)

show yield behavior. At this point, model predictions indicate that the majority of the grains have become plastic and accordingly the lattice strain response is again linear with increment in applied stress, although with slightly different gradients to that seen in the elastic regime. The origin of the plastic anisotropy comes from the anisotropy of slip in an *fcc* crystal structure. In *fcc* Fe (and hence in steel) slip occurs on the {111} planes and in the <110> directions. The analysis of the impact of this fact on the deformation of single crystals is well documented in text books (e.g., Dieter 1986), and long established; the concept is typically first met through the introduction of the Schmid factor, which in a single crystal relates the applied stress to a resolved shear stress along the particular slip system. During loading of a single crystal those slip systems that first reach the critical resolved shear stress required to initiate slip will yield first. The situation is more complicated in the case of a polycrystal and we cannot simply determine the order that differently oriented grains will reach a stress sufficient to cause yield. This is because the stress experienced by any particular grain orientation is not the applied stress, for two reasons. Firstly, due to elastic anisotropy the grains oriented, for example, with the highly elastically compliant {200} direction parallel to the applied load actually experience a lower stress than the elastically stiff {111} direction. Secondly, the surrounding grains provide a constraint resulting in a non-uniaxial stress state being experienced by any individual grain within the polycrystal aggregate. Hence to quantitatively describe the evolution of strains such as those shown in Figure 6, we require a model of polycrystal plasticity (see below).

Due to the elastic and plastic anisotropy of the individual crystallites, the presence of crystallographic texture can have an influence on the observed intergranular strains generated in the polycrystalline aggregate. Firstly, texture can alter the relative magnitude of the stresses experienced by differently oriented grain families, thereby leading to changes in how plasticity initiates in the different grain families. In *fcc* materials, where only one family of slip system operates, this effect is relatively small and is typically outweighed by the residual stresses and hardening (caused by dislocation structures) generated by the deformation which produced the texture in the first place (Daymond et al. 2000). In lower symmetry materials however, texture can have a major effect on which type of slip system can operate and hence on the internal strains generated; the effect is even more strongly evidenced when a unidirectional deformation mode such as twinning can operate (Agnew et al. 2003; Oliver et al. 2004b, 2005).

Some recent *in situ* studies have investigated the influence of cyclic loading on interphase or intergranular stresses. In this case the strain development can simply be monitored through multiple consecutive cycles (Lorentzen et al. 2002) however this ties the maximum cycling rate to the data acquisition rate and thus, given finite experimental time, the maximum number of cycles which can be studied. A greater number of cycles can be studied by interrupting rapid cyclic loading at various stages of the fatigue life to then measure the strain development around a single cycle (Korsunsky et al. 2004). Short cycle times can also be dealt with through the use of stroboscopic data acquisition techniques (Daymond and Withers 1996a) which sacrifice time resolution as a function of cycle number to increase time resolution *within* the cycle.

Finally, the intergranular strains which arise due to plasticity have been used to provide a semi-quantitative "fingerprint" of the macroscopic plastic deformation undergone by a material. The approach is to fit the differences in strains observed for the various diffraction peaks to a simple single parameter model. By comparison with calibration data, obtained for example from a uniaxial loading test, a correlation can be drawn between the single parameter fit to the diffraction data and the macroscopic plastic strain. The approach has been used for cubic and hexagonal materials with some success (Daymond et al. 1997, 1999a; Korsunsky et al. 2002).

Intergranular strains – perpendicular to the applied load

In the direction perpendicular to a uniaxially applied load, initially elastic Poisson strains are observed, with the various grain families being gradually brought into compression for an applied tensile stress. Just as each lattice plane has a different diffraction elastic constant, it will also will have a different Poisson's ratio (e.g., Daymond and Bouchard 2006). Deviations from linearity occur in the Poisson grain family strain response at applied stresses corresponding to macroscopic plasticity, however it is considerably harder to explain these nonlinearities in terms of simple "load sharing" arguments. To explain part of the reason for this, let us consider a cubic material. If we consider a (110) plane oriented with its plane normal *parallel* to the applied load, rotating the plane around the (110) normal simply alters the plane which is perpendicular to the loading direction. This has little effect on the strains which are measured in the parallel direction, since the influence is only via interaction with neighboring grains. If a sufficiently large population of grains is monitored we can expect that any effects will average out and thus the dispersion of strains in the population of grains oriented with [110] parallel to the loading direction is small. However, if the (110) plane normal is oriented *perpendicular* to the applied load, rotating about the [110] axis brings a variety of different lattice planes into alignment with the direction of loading—in fact it is possible to have either the (111)-extreme stiffness type or (200)-extreme compliance type planes oriented axially, while maintaining the [110] axis transverse to the load. The response of a given (110) plane perpendicular to the loading direction will thus be highly dependent on which plane is oriented parallel to the loading direction; in fact this can affect both the elastic Poisson and the plastic response of the observed diffraction peak (Oliver et al. 2004a). This effect was also observed in model calculations (Clausen et al. 1998) which predicted, for *fcc* materials, firstly a larger standard deviation of the perpendicular lattice strain response than of the parallel lattice strain in the elastic regime for elastically anisotropic materials, and secondly a drastic increase in the standard deviation of the perpendicular lattice strain in the plastic regime for both elastically isotropic and anisotropic materials. Thus the dispersion of strains in the direction perpendicular to the applied load is very large, and will be highly dependent on the exact population of grains present. Some subsets of the grain population may actually show a decrease in the transverse compressive strain, possibly even becoming tensile in the transverse direction (Oliver et al. 2004a) for an applied tensile stress. Even a small weighting of one level of grain orientation over another, e.g. preferred (111 parallel, 110 perpendicular) over (200 parallel, 110 perpendicular) will alter the mean strain observed in a diffraction peak perpendicular to the applied load. Both experimental and model results will be sensitive to this, because a relatively small number of grains contributed to a given diffraction peak.

In order to address these complexities in interpreting strains occurring in directions away from the primary loading axis, a number of authors have started to measure—in analogy to texture measurements—"strain pole figures" where the strain of a given reflection is measured for all orientations in a sample (e.g., Larsson et al. 2004). Some authors have gone further and calculated a "stress orientation distribution function" (SODF) based on such strain pole figures (Wang et al. 2003). However, because of the extra complexity compared to texture measurements (since a strain tensor must be determined, not just a crystal orientation), it is necessary to use some model of how strain is distributed between differently oriented grains in order to calculate the SODF, and it is thus not a direct experimental measure; Wang et al. (2003) use an elastic Eshelby model (see below).

MODELING OF PHASE INTERACTIONS AND INTERNAL STRESSES

Elastic models

Bulk aggregate properties. The evaluation of mean elastic properties for polycrystals or multi-phase materials is one of the more important problems in micromechanics and several approaches have been used over the years. Some of the more significant ones are discussed below. The key issue is one of determining the response of the aggregate, based on the properties of its constituent phases or grains. For engineering materials the drive is typically the desire to design optimum material (composite) properties for a given application. For geological materials it may be because we have made measurements on a multiphase system which has a particular geometric microstructure and wish to apply the results to a differently structured system. A number of models of varying complexity have been developed to model either the "bulk" properties based on the properties of the constituent phases, or of interpreting the behavior of constituent phases obtained by measurement.

In the Voigt (1910) approximation, in a composite body subjected to a stress at its boundaries all the composite elements (whether they are phases or grains with different orientations) are subjected to the same uniform strain, which is thus the macroscopic composite strain. We then expect obtain stress discontinuities at the boundaries of phases. In contrast, in the Reuss (1929) approximation it is assumed that the stress in the phases of the composite material is equal to the average stress applied to the material, resulting in strain discontinuities at phase boundaries. Using these approaches it is possible to develop expression for the bulk elastic properties, based on those of the constituent phases, see Simmons and Wang (1971) or Fitzpatrick and Lodini (2003). However these models are typically considered only as bounds for the real behavior since, based on energetic grounds (Hill 1952), they represent the extremes for a purely elastically deforming material. Nonetheless, for the determination of composite properties, where the constituent phases are elastically isotropic, they are easy to use and the aggregate modulus of a composite can be very simply determined. The so called "Hill-Neerfield average", which is obtained by taking the arithmetic mean of the Reuss and Voigt approaches is often used as a first estimate of material behavior for approximately isotropic systems (e.g., Noyan and Cohen 1987), and is typically found to be in good agreement with more complex models, at least in the case of untextured polycrystals.

Hashin and Shtrikman (1962, 1963) have also derived elastic properties for multiphase materials, making no prescriptions about the geometry of the phases, assuming only that the individual phases are isotropic, homogenous and well distributed. They defined the elastic behavior of the material in terms of the strain energy stored in the material subjected to uniform strains or stresses. By minimization of either potential or complementary potential energy under suitable constraints, two bounds on behavior can be produced which are more restrictive than the Voigt / Reuss limits. The Hashin and Shtrikman model is often used to check more complicated models' predictions of the elastic moduli of multi-phase systems

because, since the model is generally to be considered to come close to the limit of how closely the two bounds for composite behavior can be brought when the only given information is elastic properties and volume fraction. The Hashin and Shtrikman bounds for isotropic materials are:

$$K_{HS} = \left\{ \sum_i \frac{c_i}{3K_i + 4\mu} \right\}^{-1} \sum_j \frac{c_j K_j}{3K_j + 4\mu} \tag{13}$$

$$\mu_{HS} = \left\{ \sum_i \frac{c_i}{6\mu_i(K + 2\mu) + \mu(9K + 8\mu)} \right\}^{-1} \sum_j \frac{c_j \mu_j}{6\mu_j(K + 2\mu) + \mu(9K + 8\mu)}$$

where c_i is the volume fraction of the i^{th} phase (or grain family), K_i and μ_i are the bulk and shear modulus of the i^{th} phase respectively and:

if $K = \max\{K_i\}$, $\mu = \max\{\mu_i\}$ we obtain the upper bound

but if $K = \min\{K_i\}$, $\mu = \min\{\mu_i\}$ we obtain the lower bound.

The Young's modulus can be calculated from K and μ for either bound using the conventional isotropic relation:

$$E_{HS} = \frac{9K_{HS}\mu_{HS}}{3K_{HS} + \mu_{HS}} \tag{14}$$

For example, the elastic response of an approximately equi-volume olivine-magnesiowüstite composite under uniaxial compression has been shown to lie within relatively tight Hashin and Shtrikman bounds (Fig. 7), based on neutron diffraction measurements of the internal strains borne by each phase (Schofield et al. 2003). Covey-Crump et al. (2006b) have shown how the strain borne by the phases in a halite-calcite composite, starts off roughly equidistant between the Voigt and Reuss limits during initial loading, and then deviates from linearity tending towards the Voigt limit as plasticity occurs in the halite phase (Fig. 8). The initial formulation was later extended (Watt 1980; Watt and Peselnick 1980) to materials of lower symmetry (except triclinic) for which, naturally, rather more complex versions of Equation (13) arise.

Both the advantage and disadvantage of the modeling approaches given above is that no description of the microstructure is included. Many more complicated models which do take into account geometrical arrangements have been developed in the prediction of composite elastic properties; some such as e.g., the Shear Lag Model are reviewed in Clyne and Withers (1993), while others, such as the Eshelby model, are discussed in the context of composites below.

Diffraction elastic constants. While the determination of average aggregate properties based on individual components is an important area of study, the calculation of diffraction elastic constants (i.e., the plane specific Young's modulus) from the single crystal elastic stiffnesses is of great interest to the diffraction community. The same models described in the previous section can be applied to this task. For example, for the Voigt model we see that all grains in the polycrystal aggregate will experience the same strain (which must be the average strain), hence all *hkl* orientations will have the same lattice strain in a given direction, and thus the moduli can be found by the approach given in the previous section. For the Reuss model, since all grains experience the same (applied) stress, the appropriate elastic modulus is simply that described in Equation (9). The same modeling approaches can also be employed to determine the appropriate modulus in the Poisson's direction (e.g., Noyan and Cohen 1987).

The most common model used in the calculation of diffraction elastic constants of untextured polycrystalline materials however is the Kröner (1958, 1961) model. This approach

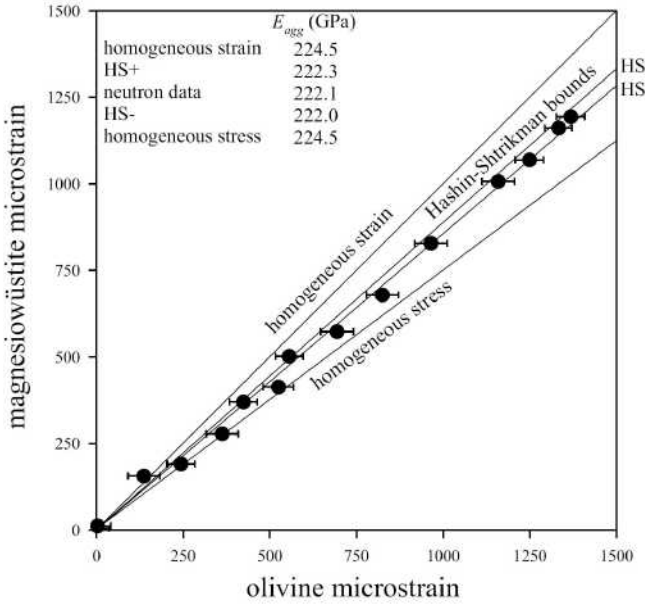

Figure 7. The relationship between the phase average elastic strains parallel to the direction loading, of the phases of an elastically isotropic 54% olivine + 46% magnesiowüstite composite during elastic deformation, from Schofield et al. (2003). Also shown are the theoretical bounds on the behavior predicted by homogeneous stress (Reuss) and homogeneous strain (Voigt) conditions, and the Hashin-Shtrikman bounds, which the neutron diffraction data lies between.

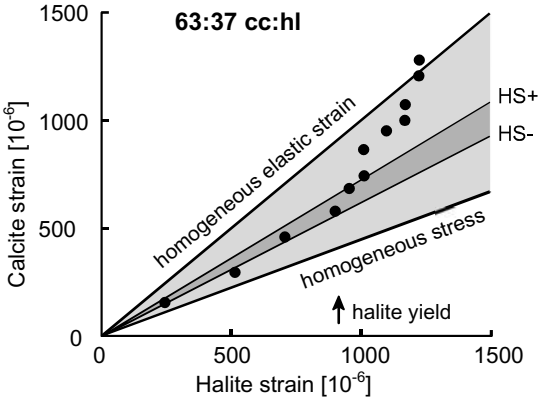

Figure 8. Comparison of the calcite and halite phase average strains parallel to the direction of loading at various increasing applied stresses, for a 63% calcite/37% halite (by volume) composite. Also shown is the strain partitioning predicted during the elastic phase of the deformation assuming homogeneous stress (Reuss) and homogeneous strain (Voigt), and the region that lies between the Hashin-Shtrikman (HS±) bounds. While deformation is elastic, the system is well described by the HS bounds, but once plasticity occurs in the halite, deviation from linearity occurs indicating load redistribution from the halite to the calcite phase. [Used wtih permission from Elsevier, from Covey-Crump et al. (2006b), Fig. 1b.]

utilizes the Eshelby approach (see below) so is often also referred to as a self-consistent analysis. By assuming random texture and spherical grains it is possible to derive analytic expressions for the diffraction elastic constants. These expressions are relatively complex, for example see Fitzpatrick and Lodini (2003). Here just the final result for cubic symmetry materials is given:

$$G^3 + \alpha G^2 + \beta G + \gamma = 0 \tag{15}$$

where

$$\alpha = (9A_1 + 4A_2)/8$$
$$\beta = A_2(3A_1 + 12A_3)/8$$
$$\gamma = 3A_1A_2A_3/8$$
$$1/A_1 = 3(S_{11} + S_{12}); \qquad 1/A_2 = S_{44}; \qquad 1/A_3 = 2(S_{11} - S_{12})$$

The solution to Equation (15) is substituted into Equation (16):

$$E_{hkl} = \frac{\omega}{1 - 2\omega(1 - 5A_{hkl})t_{44}}; \qquad \nu_{hkl} = \frac{2G\left[1 + \omega(1 - 5A_{hkl})t_{44}\right] - \omega}{2G\left[1 - 2\omega(1 - 5A_{hkl})t_{44}\right]} \tag{16}$$

where A_{hkl} is given by Equation (10) and

$$t_{44} = \frac{(G - A_2)(3A_1 + 6G)}{2G\left[8G^2 + G(9A_1 + 12A_2) + 6A_1A_2\right]}; \qquad \omega = \frac{9A_1G}{3A_1 + G} \tag{17}$$

The anisotropy of the individual crystallites means that texture *does* have an effect on the observed diffraction elastic constants. Thus, more recently, in order to determine diffraction elastic constants workers have employed Finite Element crystal plasticity approaches (Wern et al. 2002), or self-consistent approaches (see below) which are more complex than the Kröner model. Such models have the advantage of being able to include the influence of texture on elastic properties, but the disadvantage of requiring numerical solution.

The reverse problem—determining the single crystal elastic constants given the measured polycrystal diffraction elastic constants—is tractable using appropriate modeling techniques. This reverse approach to calculating the single crystal stiffness is particularly important for many engineering systems e.g., TiAl where single crystals of sufficient size for individual testing simply cannot be fabricated. A similar issue would also arise for many geological materials. The results obtained by such methods match reasonably well with other reported data when alternative approaches are used. However, it should be noted that the results are sensitive to the quality of the data and the details of the modeling approach used. Using an appropriate approach is particularly important when the polycrystal exhibits texture. Dealing with this problem is outside of the scope of this paper; readers are referred, for example, to the review of techniques appropriate for untextured materials given in (Gnaeupel-Herold et al. 1998), and for a rigorous approach to dealing with the reverse problem in the case of textured materials to (Matthies et al. 2001). Some simple approaches are also described in (Howard and Kisi 1999).

Inelastic models

Composite models - Eshelby model. A number of avenues have been explored in attempting to include the effect of phase/grain geometry on the mechanical properties of polycrystalline materials, one of the most successful being the Eshelby or Mori-Tanaka method (Eshelby 1957, 1959; Mura 1987), where inclusions (phases or grains) are modeled as ellipsoids. The approach is to consider the elastic field about a single inclusion in an infinite isotropic matrix of the same elastic constants. The inclusion is "cut" from the unstressed matrix and then allowed to undergo a stress-free shape change. Its surface is then stressed such that it can be replaced and

"welded" (i.e. no interfacial sliding allowed) into the original hole from which it was cut. The constraints are then removed, and an equilibrium with the matrix is attained when the inclusion reaches a particular strain. By building up combinations of such shape changes it is possible to simply model elastic and thermal loading of the matrix and inclusion. While such an exercise can be carried out for an arbitrarily shaped inclusions, Eshelby showed that in the special case of ellipsoidal inclusions, an analytical solution is possible. Since ellipsoids can, dependent on aspect ratio, vary from cylinders, to spheres to flat discs, this gives great flexibility in modeling composites. The approach has been used with considerable success in modeling composite mechanics. An accessible review of the method, including its application to the deformation of composites, and comparisons with neutron diffraction strain measurement is given by Withers et al. (1989). The Eshelby method has also been developed extensively e.g., to take account of arbitrary elastic anisotropy of the inclusion and of the host material and for porous elasticity (Levin and Alvarez-Tostado 2003).

As well as the obvious advantages of using the Eshelby technique for modeling elastic properties of composites which are gained from the fact that it incorporates the phase geometry in a simple manner, considerable success has also been achieved using various adaptations of the method to model plasticity in composites (Clyne and Withers 1993). For example Fitzpatrick et al. (1997; 2002) have shown how it is possible to use the internal strains measured by diffraction, in combination with the Eshelby method to separate out thermal, elastic and plastic contributions to the observed response of a two phase composite where one phase is elastic.

Composite models - finite element models. Finite element modeling has been shown to be an extremely powerful tool for investigating load sharing between phases in a composite. In this case, the microstructure of the composite is modeled using a finite element mesh, where the properties of the mesh are varied spatially to match the appropriate elasto-plastic properties of the composite. While a few attempts (e.g., Brockenbrough et al. 1991) have been made to model particular microstructures (by digitizing of actual micrographs) it is in particular the unit cell approach which has had greatest success. In this approach, the random distribution of phases is modeled as some uniform regular array, which can then be approximated using a unit cell approach, i.e., modeling a single reinforcement, but with boundary conditions that are appropriate to mimic an infinite regular array (e.g., Levy and Papazian 1990). This has obvious computational advantages, and seems to be a reasonable approximation in many cases. For example; Daymond et al. (1999b) have used the technique to interpret the shift from plasticity to creep on raising the temperature of Cu-Mo, and to separate the relative contributions of creep and plasticity in the deformation of a thermally ratcheting Al-SiC composite (Daymond and Withers 1996a), while Agrawal et al. (2003) used it to study the generation of tensile stress at the interface of a co-continuous Cu-Al_2O_3 composite due to thermal misfit strains.

Polycrystal plasticity models – Taylor and Sachs. Two of the simplest models for dealing with polycrystalline plasticity developed by Taylor (1938) and Sachs (1928) are—despite their age—still used. The Taylor (1938) model is analogous in many ways to the Voigt model for elasticity; the crystals are treated as rigid-plastic (i.e., no elastic deformation) and plastic strain is assumed to be homogenous, irrespective of grain orientation; this strain is equal to the average strain. The same assumption is made for strain rate. Thus stress is discontinuous across boundaries. In particular, it has been used with considerable success in the prediction of texture development in metals. The determination of yield in a grain is controlled by the usual Schmid relationship. In the Sachs (1928) model on the other hand, rigid plastic grains are assumed to all have the same stress, thus having strain discontinuities at grain boundaries. It is usually considered a lower bound for polycrystal models, while the Taylor model is considered an upper bound. Since these models treat grains as rigid plastic, neither are particularly appropriate to the study of internal strains in materials.

Based on the Eshelby method (described above) more complex schemes were introduced by Kröner (1961) and Budiansky and Wu (1962) and were significant advances in that, unlike the Sachs and Taylor models, they included the elastic anisotropy of the material. The approach taken was to model grains in the polycrystal as ellipsoids in an infinite medium. The medium has the average properties of the population of grains. No direct grain-to-grain interaction is accounted for—all interaction is accounted for via the medium properties. The coupling between the grains and the medium was modeled as purely elastic, and resulted in very low deformation heterogeneity. A significant advance was made by Hill/Hutchinson (next section) who then introduced an elasto-plastic coupling between grain and medium.

Polycrystal plasticity models – Hill/Hutchinson. As suggested in the description of the origin of Type II intergranular strains in steel and aluminum, if we are to explore the different responses of the variously oriented grain families, i.e., to understand the behavior of the individual diffraction peaks and the intergranular strains, we need a description which captures the interaction of the elastic and plastic properties of the polycrystalline aggregate. A popular approach in recent years has been the Hill (1965) self-consistent approach, first implemented by Hutchinson (1970). In this model a population of grains is chosen with a distribution of orientations and volume fractions that match the measured texture. Each grain in the model is treated as an ellipsoidal inclusion and is attributed anisotropic elastic constants and slip mechanisms characteristic of a single crystal of the material under study. Interactions between individual grains and the surrounding medium (which has properties of the average of all the grains) are performed using an elasto-plastic Eshelby (1959) self-consistent formulation. Since the properties of the medium derive from the average response of all the grains, it is initially undetermined and must be solved by iteration. Small total deformations are assumed, and usually no lattice rotation or texture development is incorporated. A number of groups have developed such models, some with slight modifications and developments compared to that described by Hutchinson. Details of the implementation of two examples of these more recent models can be found in Turner et al. (1995) and Clausen et al. (1998). Such models are typically termed elasto-plastic self-consistent (EPSC) models.

The single crystal elastic constants used in the model may be taken from the literature values, however there may be some variation with alloying (Dawson et al. 2001). Thus, the values are typically verified by comparison to the elastic experimental data, or if sufficiently high quality measurements are collected they can be calculated directly from the data in the elastic regime (e.g., Matthies et al. 2001). Considering the plastic flow law, the critical resolved shear stress and exponential hardening coefficients used are various, but in many calculations, an extended Voce law (Tomé et al. 2001) is used:

$$\tau = \tau_0 + \left(\tau_1 + \theta_1\Gamma\right)\left(1 - \exp\left[\frac{-\theta_0\Gamma}{\tau_1}\right]\right) \tag{18}$$

where Γ is the accumulated shear strain in the grain. The crystallographic shear flow stress τ in Equation (18) describes (in an average way) the resistance to activation that the deformation modes experience. The threshold value is τ_0, and it usually increases with deformation due to strain-hardening, which is here shown to follow a modified Voce law; τ_1 is the Voce stress where the hardening extrapolates to a zero value of accumulated shear and θ_0 is the athermal initial hardening rate (Kocks et al. 1998; Kocks and Mecking 2003). The final hardening rate θ_1 can be non-zero. Typically the hardening parameters in Equation (18) are fitted to give optimum agreement with the macroscopic stress-strain curves, since while single crystal values can be determined explicitly, the actual values found in the polycrystal are influenced by grain size, dislocations, precipitates etc.

Plastic slip is assumed to take place on the appropriate slip systems, for example for *fcc* crystal structures the twenty-four <110> {111} systems. The same set of yield and hardening

values are initially applied to all systems and grains (i.e., for *fcc* structures there are only four fitting parameters in the model for a given test). However each individual slip system in a given grain is subsequently kept track of during modeling of the deformation, and the hardening curve followed appropriately according to the accumulated shear strain.

In order to provide reasonable comparisons with diffraction data a subset of the total population of grains used in the model is identified for each diffracting family, as defined by the condition of having an *hkl* plane-normal lying within, for example, a 5° cone around the nominal scattering direction. In many cases the angular span can be chosen to match the actual detector coverage used in the experiment. A population of grains is chosen to represent the texture—typically this might be of the order of 1000 to 5000 appropriately weighted grains (see below for further discussion as to required grain populations).

This model has been shown to be in good to excellent agreement in comparison with diffraction data for a range of metals, including *fcc* (Pang et al. 1998b; Clausen et al. 1999), *bcc* (Pang et al. 1998a; Daymond and Priesmeyer 2002), and *hcp* (Turner and Tomé 1994; Pang et al. 1997; Daymond and Bonner 2002) crystal structures. An example indicating the level of agreement which can be obtained is shown in Figure 9. A number of important issues remain in the implementation of these models, most significantly the way that interactions between the grain and matrix are fine tuned (e.g., Tomé 1999), and the way that interactions between different slip systems, i.e. latent hardening (Xu et al. 2006), are handled. Attention has also been applied more recently to the study of multiphase systems, where the interphase and intergranular stresses will superimpose in some manner (e.g., Gharghouri et al. 1999; Dye et al. 2001; Daymond and Priesmeyer 2002; Daymond et al. 2005; Daymond and Fitzpatrick 2006)

Polycrystal plasticity models – crystal plasticity finite element models. The other major class of model used to describe polycrystal plasticity is the finite element approach. In the

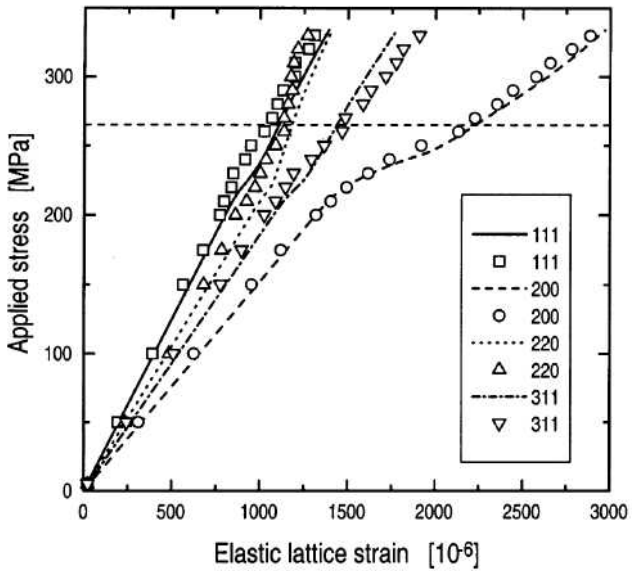

Figure 9. A comparison between experiment and EPSC model data for applied stress versus the elastic lattice strains parallel to the applied stress for several diffraction peaks in *fcc* steel. Experimental data corresponds to that shown in Figure 6. Symbols are measured and lines are calculated. The horizontal dotted line represents the macroscopic 0.2% yield limit. [Used with permission of Elsevier from Clausen et al. (1999), Fig. 5a.]

crystal plasticity finite element (CPFE) approach, a finite element mesh is used to represent a polycrystalline aggregate. This is different from the composite unit cell model when, typically, only two phases are modeled. In CPFE the constitutive behavior varies spatially over the FE mesh to a much greater extent, with the local mesh behavior chosen to simulate the elasto-plastic behavior of an aggregate of many single crystals. The method was originally developed for the prediction of texture evolution where it has proven extremely effective e.g. (Dawson and Marin 1998), and has more recently been applied to model the elastic strain response of grains during plastic deformation and compared with diffraction results e.g. (Dawson et al. 2001). The great advantage of the CPFE method is that it can explicitly account for the influence of neighboring grains, local neighborhood and grain-to-grain interaction. The major disadvantage of the CPFE method is the high computational overhead required to simulate a significant number of grains. For the calculation of mean grain family elastic strains, the CPFE method is of the order of 100 times slower than EPSC for the same grain population (Fonseca et al. 2006). Further, since nearest neighbor effects are explicitly accounted for in CPFE, this means that typically it is necessary to model a larger population of grains to get a reasonable polycrystal average than in the EPSC case. This therefore means that it is likely that while EPSC and CPFE approaches will agree well in predicting *average* elastic strain in a particular grain family, the *distribution* of strain around this mean is likely to be better physically represented by the CPFE approach than by the EPSC model, although to date there have been only one direct quantitative comparison between the approaches (Fonseca et al. 2006). While a large body of CPFE publications exist, with relevance to comparisons with neutron diffraction strain measurement, the work of Dawson et al. (2001, 2005) and Bate and Fonseca (2004) should be noted. Particular success has been achieved in the study of Al and in other cubic alloys. Some recent studies have considered mixed finite element—crystal plasticity models, whereby the FE code is used to model spatial variation while a (non-FE) crystal plasticity code model is used to provide the constitutive law for the FE model. Such multiscale models have been developed either using a decoupled (Tomé et al. 2001; Oliver et al. 2004a) approach, where the crystal plasticity code is run separately to the FE code, via a "look-up table", as well as through true coupled (Raabe et al. 2002; Daymond 2005) approaches, where the crystal plasticity code is embedded into the FE code.

Further examples of the use of polycrystal plasticity models to interpret deformation

Twinning and domain reorientation. While the intergranular stresses which develop during plastic deformation of *fcc* metals thus seem at least reasonably well understood, the trends of internal stress generation in lower symmetry materials are less well characterized. Part of the reason for this is that typically multiple deformation modes can potentially operate (e.g., basal slip, prism slip) in such materials. Further, observations vary considerably between different materials due to the sensitivity of the different deformation modes to factors such as unit cell aspect ratio, grain size and temperature. In addition, in some materials it is well known that mechanical twinning can be an important deformation mechanism. Since twinning is a unidirectional shear mechanism, in highly textured materials complex interactions between twinning and slip can occur depending on the sense of the imposed load relative to the texture (e.g., Kaschner et al. 2006). Since twinning is associated with an actual crystallographic rearrangement, as well as with changes in strain, twinning is associated with a change in intensity of diffraction peaks. A number of neutron diffraction studies of internal strain generation have been carried out on a range of materials that undergo twinning—predominantly *hcp* materials such as alloys based on Zr (Turner et al. 1995), Be (Brown et al. 2003), Mg (Gharghouri et al. 1999; Agnew and Duygulu 2005) and Ti (Cho et al. 2002), all of which have important technological applications. For example, Gharghouri et al. (1999) used their neutron diffraction results to suggest that both $\{10\bar{1}1\}$ and $\{10\bar{1}2\}$ twinning must be active modes in their particular Mg alloy. Such twinning reorientations in metals are highly analogous to the domain switching that occurs in a whole class of ferroelectric/ferroelastic ceramics (e.g., Cain

et al. 1994; Rogan et al. 2003) and which been successfully studied using diffraction. Indeed, in some ways these are simpler systems to interpret than metals, since the domain switching is expected to be the only deformation mechanism present. For example, Rogan et al. (2003) were able to demonstrate and quantify the different amounts of domain switching occurring in each phase of two phase $Pb(Zr,Ti)O_3$ (i.e., where both rhombohedral and tetragonal forms are present) under mechanical loading. Such mechanical twinning is also highly relevant to the study of a range of minerals, most obviously calcite, quartz and spinels.

Effect of temperature. By probing the internal stresses during deformation as a function of temperature using neutron diffraction, and comparing the results obtained with micromechanical models, it is possible to elucidate the effect of temperature on mechanisms. For example, Daymond et al. (1999b) studied the influence of raised temperature on the internal stresses generated in a Cu-Mo particulate composite, interpreting the observed strains using a unit cell finite element model and demonstrating the influence of local creep diffusion as the temperature was raised. An example of the study of the influence of temperature on intergranular strains in an *fcc* stainless steel is given in (Daymond and Bouchard 2006). A slip based polycrystal plasticity model was in good agreement with the experimental data up to 0.4 of melting point (T_m). By 0.49 T_m the model was still in reasonably good quantitative agreement, but by 0.55 T_m agreement was at best qualitative. Oliver et al. (2004b) have examined the influence of temperature on the relative contributions of slip and twinning modes as a function of temperature in a magnesium alloy; this is significant because the critical resolved shear stress required for twinning is much less temperature sensitive than that for slip.

Phase transformations. Neutron diffraction has long been used for the study of phase transformations, i.e. where the crystallographic phase changes either by a diffusive or displacive mechanism. Particular interest in the crystallography physics community has focused on transformations caused either by a change of temperature (Redfern 2006, this volume) or magnetic field (Von Dreele 2006, this volume). Geologists have used the technique to study the influence of pressure (Parise 2006, this volume). Given the plethora of work we give a few example here of those studies where internal stresses have specifically been of interest. Particularly with relevance to engineering applications, there has been much work on Shape Memory Alloys (SMAs). These are an important class of engineering materials in that the phase transformations are affected by both temperature and stress, making them potentially useful in a range of actuator and sensor applications. Due to the highly non-linear nature of their response, there is a strong drive to obtain models to assist in their implementation in engineering design. SMAs owe their unusual mechanical behavior to a martensitic transformation. The advantage of studying the transformation using neutron diffraction is that, by suitable analysis of the data, it is possible to determine the volume fraction, the preferential selection of crystallographic variants or orientations (Wenk 2006, this volume) and the development of internal strains, as the transformation progresses as a function of applied load (see Fig. 10). Examples of such studies, include work on NiTi (Vaidyanathan et al. 1999), CuAlZnMn (Šittner et al. 2002) and FePd (Oliver et al. 2003). For example, Oliver et al. (2003) showed that internal stresses played a significant role in driving the reversal of martensite variant changes when the applied stress was removed. Other examples of studies of the interaction of internal stresses with phase transformations include studies on steels (Oliver et al. 2002) and ceramics (Üstündag et al. 1995).

Particular application of the techniques to geological materials and systems

Engineers have long sought to develop constitutive models for material behavior which can be applied in predicting the performance and lifetime of components. There is a direct analogy here with those working in rock mechanics, who require such models to describe the elastic and plastic properties of geological materials, though admittedly the length scales and timescales are somewhat different. Thus, an understanding of the elastic properties of rocks plays an important role in the interpretation of seismological data, while models of the plastic and visco-plastic

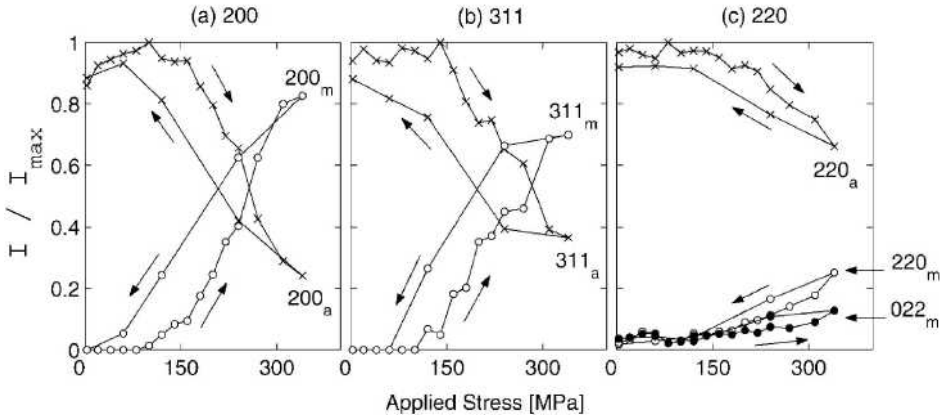

Figure 10. Variation of integrated peak intensities with applied stress in the direction parallel to the applied stress, during stress-induced transformation at 24 °C in FePd. Crosses are austenite diffraction peaks; circles are martensite diffraction peaks with the same Miller indices, as labeled for each plot. Intensities are normalized with respect to the maximum intensity of the appropriate austenite reflection. Arrows indicate the loading and unloading curves. [Used wtih permission of Elsevier from Oliver et al. (2003), Fig. 6.]

properties are applied in the thermo-mechanical modeling of the lithosphere (Schofield et al. 2003). It should be emphasized that the majority of systems that are of interest to geologists are in fact composite structures (polymineralic rocks) which thus have mechanical properties dependent on the individual phases, and the geometric arrangement of these phases and their interfaces. The ability to predict the behavior of such composites based on the properties of their constituent phases would thus be of great significance. The application of the techniques described above, which have been well established in the study of engineering materials to geological systems is relatively new, but a small number of studies are in the literature.

Pintschovius et al. (2000) considered the residual stresses resulting from the plastic deformation of monomineralic rock—demonstrating that even quite small stresses could be successfully measured. *In situ* studies of the loading of monomineralic rocks have looked at the elastic response of different diffraction planes (Scheffzük et al. 1998) as well as the effect of microcracking on the response of diffraction planes under nominally elastic loading (Meredith et al. 2001). The techniques described earlier in this paper have been applied to spatial mapping studies of Type I stresses (e.g., Meredith et al. 1997), and their variation near a previously shock loaded interface (Scheffzük et al. 2005). An interesting group of studies considering the elastic strain partitioning in polyphase rocks (Frischbutter et al. 2000; Covey-Crump et al. 2001, 2003) have demonstrated the limits of validity of the simple elastic models detailed in this paper in describing the phase response. Some of this work is reviewed by Schofield et al. (2003). Darling et al. (2004) used neutron diffraction to examine the internal strain state in sandstones which exhibit a non-linear, hysteretic relation between stress and macroscopic strain (i.e., measured by an extensometer). Whilst without a constraining pressure or elevated temperature (or both) the possibility of studying plasticity in geological systems is limited to certain materials systems such as halite, there has been some initial work in this area (Covey-Crump et al. 2006b). Recent work has looked at the way that introducing a confining pressure can further widen the scope of *in situ* loading studies (Dobson et al. 2005; Covey-Crump et al. 2006a). Finally, "man-made" rocks are also susceptible to theses techniques with, for example, Schulson et al. (2001) using neutron diffraction to monitor the development of internal strain within the calcium hydroxide phase of hardened Portland cement paste as the material cooled, with the effect attributed to the thermal mismatch between calcium hydroxide and calcium silicate hydrate phases.

There are a number of complexities which need to be considered when we are considering making measurements on geological systems, compared to the wide range of studies on engineering materials. We summarize these aspects here; some are discussed in more detail by Schofield et al. (2003).

Grain size. Typical studies of polycrystalline materials have assumed that a powder approximation can be made, that is sufficient grains/crystallites are present in the diffracting volume to be able to use statistical arguments in interpreting the deformation. Recent developments at neutron and in particular synchrotron X-ray facilities have pushed the techniques towards the study of a small number of individual grains (Martins et al. 2004), but this area of research is still in its infancy in terms of providing data for direct comparison and validation of models. Putting an exact figure on the number of grains that should be present in the measurement volume is not simple, since it will depend on the characteristics of the diffraction instrument, and in particular on the divergence of the incident beam and the angular coverage of the detector, both of which affect how many of the grains in the volume will contribute to the diffraction pattern. Based on model observations, it is typically considered that several thousand grains are required in the gauge volume for results to be reasonably statistically significant—typically 1% or less of the grains within the measurement volume will contribute to the diffraction signal. Hence obtaining results that are statistically meaningful requires many grains, with Clausen et al. (2003) suggesting around 10,000 based on their modeling studies. Reliable diffraction measurements are usually carried out on several hundred thousand grains. Geological materials often have large grain sizes which may complicate this requirement, particularly for spatial mapping studies. In such cases techniques to increase the number of grains which can contribute are often employed, for example carrying out a small angular "rocking" of the sample about the principal measurement vector, or spatial scanning along an axis where no strain variation is expected. If a smaller number of grains are present, it may still be possible to carry out measurements, but a significantly increased scatter is likely to be observed in the results due to the variation in number of sampled grains, and hence to the significance of local neighborhood on the measured strains.

Crystal structure and symmetry. Geological materials often have a low symmetry, compared to many engineering materials which are either cubic or hexagonal. This reduced crystal symmetry results in an increase in the number of peaks—in extreme cases such as monoclinic very few fully separate (i.e., non-overlapping) peaks are available, making a multipeak analysis preferable. Further it should be noted that a decrease in symmetry increases the required count times, although this is not particularly significant in comparison to the long count times experienced for some Ti and Co based engineering alloys due to the particular neutron scattering/absorption properties of these materials.

When crystal structures are very close, such as ortho- and clino-pyroxenes, the similar structures result in very similar diffraction patterns. As the diffraction patterns become more and more similar, distinguishing the phases requires higher resolution instruments and increased data collection times. However, even when phases are close together in structure, advanced data analysis strategies can be employed in some cases (e.g., Stone et al. 1999). Similar problems with peak overlap and difficulty in distinguishing phases may occur if many phases are present, or phases are present in very small quantities. Typically measurement will not give accurate strains if less than a few percent by volume of a phase is present (unless its scattering is significantly stronger than the other phases). If more than four or five phases are present, one would also expect significant overlap in the diffraction patterns which would make separating out the elastic strains in the individual phases difficult. However, it should be noted that quite typically a measurement accuracy in strain of 10^{-4} and sometimes 5×10^{-5} is obtained. For an atomic lattice of 0.3 nm, this corresponds to monitoring the average atomic lattice spacing to an accuracy of better than 0.03 pm.

Elemental issues. Unlike X-rays which have scattering that decreases more or less monotonically as atomic number increases, the scattering of neutrons varies—for our purposes—more or less randomly across the periodic table (Bacon 1975). Of particular note H has a very large incoherent scattering (i.e., creates a significant background signal), while the presence of isotopes of certain elements most noticeably Gd, B and Cd cause significant neutron absorption. If significant quantities of these elements are present in the material it is not possible to transmit neutrons through more than a small thickness of material.

CONCLUSIONS

Neutron diffraction is an extremely effective probe for the measurement of internal stresses in polycrystalline materials. Measurements of diffraction peak position can be correlated to changes in the lattice parameter and hence interpreted as an elastic strain. With a knowledge of the appropriate elastic stiffness, stress can be calculated from these strains. The changes in stress state, in particular its variation between phases or as a function of crystallographic orientation allow an interpretation of the deformation mechanisms that are operating. Models of polycrystal deformation are particularly helpful in interpreting such experimental data.

The techniques of strain measurement by neutron diffraction and synchrotron x-ray diffraction have thus been extensively used in the study of engineering materials. They have led directly to insights into the influence of processing methods on residual stress development and into the interpretation of deformation mechanisms operating in materials. There seems considerable potential for the techniques to be applied to geological materials, an area that is at present just starting to be explored.

ACKNOWLEDGMENTS

This work has benefited greatly from various collaborations and interactions with my colleagues. In particular I would like to thank Dr. Mike Fitzpatrick, of the Open University, UK, and the manuscript reviewers for useful comments on the Chapter. In addition, many members of the neutron diffraction stress measurement community worked together closely in the period 1996-2001 under the auspices of VAMAS TWA-20, resulting in the publication of an ISO Technology Trends Assessment (Webster 2001). This Chapter incorporates the recommendations made by that group.

This work benefited from the funding provided by the Canadian National Science and Engineering Research Council, and by the Canadian Foundation for Innovation through a Canada Research Chair in Mechanics of Materials.

REFERENCES

Agnew SR, Duygulu O (2005) Plastic anisotropy and the role of non-basal slip in magnesium alloy AZ31B. Int J Plasticity 21:1161-1193

Agnew SR, Tome CN, Brown DW, Holden TM, Vogel SC (2003) Study of slip mechanisms in a magnesium alloy by neutron diffraction and modelling. Scripta Mater 48:1003-1008

Agrawal P, Conlon K, Bowman KJ, Sun CT, Cichocki FR, Trumble KP (2003) Thermal residual stresses in co-continuous composites. Acta Mater 51:1143-1156

Allen AJ, Bourke M, Dawes S, Hutchings MT, Withers PJ (1992) The analysis of internal strains measured by neutron diffraction in Al/Sic metal matrix composites. Acta Metall Mater 40:2361-2373

Bacon GE (1975) Neutron Diffraction, 3rd ed. Oxford

Bate PS, Fonseca JQd (2004) Texture development in the cold rolling of IF steel. Mater Sci Eng A 380:365-377

Bollenrath F, Hauk V, Müller EH (1967) On calculation of polycrystalline elasticity constants from single crystal data. Z Metallkd 58:76-82

Bourke MAM, Goldstone JA, Shi N, Allison JE, Stout MG, Lawson AC (1993) Measurement and prediction of strain in individual phases of a 2219Al/TiC/15p-T6 composite during loading. Scripta Mat 29:771-776

Brockenbrough JR, Suresh S, Wienecke HA (1991) Deformation of MMCs with continuous fibers: geometrical effects of fiber distribution and shape. Acta Metall Mater 39:735-752

Brown DW, Bourke MAM, Clausen B, Holden TM, Tome CN, Varma R (2003) A neutron diffraction and modeling study of uniaxial deformation in polycrystalline beryllium. Metall Mater Trans A 34A:1439-1449

Budiansky B, Wu TT (1962) Theoretical prediction of plastic strains in polycrystals. *In: Proceedings of the 4th U. S. National Congress of Applied Mechanics,* University of California, Berkeley, California. Rosenberg RM (ed) Vol. **1**, p 1175-1185

Cain MG, Bennington SM, Lewis MH, Hull S (1994) Study of the ferroelastic transformation in zirconia by neutron-diffraction. Philos Mag B 69:499-507

Carter DH, Bourke MA (2000) Neutron diffraction study of the co-deformation behaviour of beryllium-aluminium composites. Acta Mater 48:2885-2900

Cho JR, Dye D, Conlon KT, Daymond MR, Reed RC (2002) Intergranular strain accumulation in a near-alpha titanium alloy during plastic deformation. Acta Mater 50:4847-4864

Clausen B, Leffers T, Lorentzen T (2003) On the proper selection of reflections for the measurement of bulk residual stresses by diffraction methods. Acta Mater 51:6181-6188

Clausen B, Lorentzen T, Bourke MAM, Daymond MR (1999) Lattice strain evolution during uniaxial tensile loading of stainless steel. Mater Sci Eng 259:17-24

Clausen B, Lorentzen T, Leffers T (1998) Self-consistent modelling of the plastic deformation of fcc polycrystals. Acta Mater 46:3087-3098

Clyne TW, Withers PJ (1993) An Introduction to Metal Matrix Composites. Cambridge University Press

Covey-Crump SJ, Holloway RF, Schofield PF, Daymond MR (2006a) A new apparatus for measuring mechanical properties at moderate confining pressures in a neutron beamline. J Appl Cryst 39:222-229

Covey-Crump SJ, Schofield PF, Daymond MR (2006b) Using neutrons to investigate strain partitioning between the phases during plastic yielding of calcite + halite composites. Physica B *in press*

Covey-Crump SJ, Schofield PF, Stretton IC (2001) Strain partitioning during the elastic deformation of an olivine-mangesiowustite aggregate. Geophys Res Lett 28:4647-4650

Covey-Crump SJ, Schofield PF, Stretton IC, Knight KS, Ismail WB (2003) Using neutron diffraction to investigate the elastic properties of anisotropic rocks: results from an olivine + orthopyroxene mylonite. J Geophys Res - Solid Earth 108(B2): Art. No. 2092

Darling TW, TenCate JA, Brown DW, Clausen B, Vogel SC (2004) Neutron diffraction study of the contribution of grain contacts to nonlinear stress-strain behavior. Geophys Res Lett 31:Art. No. L16604

Dawson P, Boyce D, MacEwen S, Rogge R (2001) On the influence of crystal elastic moduli on computed lattice strains in AA-5182 following plastic straining. Mater Sci Eng A 313:123-144

Dawson PR, Boyce DE, Rogge RB (2005) Correlation of diffraction peak broadening to crystal strengthening in finite element simulations. Mater Sci Eng A 399:13-25

Dawson PR, Marin EB (1998) Computational mechanics for metal deformation processes using polycrystal plasticity. Adv Appl Mech 34:77-169

Daymond MR (2004) The determination of a continuum mechanics equivalent elastic strain from the analysis of multiple diffraction peaks. J Appl Phys 96:4263-4272

Daymond MR (2005) A combined finite element and self-consistent model; validation by neutron diffraction strain scanning. Mater Sci Forum 495:1019-1024

Daymond MR, Bonner NW (2002) Lattice strain evolution in IMI 834 under applied stress. Mater Sci Eng A 340:263-271

Daymond MR, Bouchard PJ (2006) Elastoplastic deformation of 316 stainless steel under tensile loading at elevated temperatures. Metall Mater Trans A 37A:1863-1873

Daymond MR, Bourke MAM, Von Dreele RB (1999a) Use of Rietveld refinement to fit an hexagonal crystal structure in the presence of elastic and plastic Anisotropy. J Appl Phys 85:739-747

Daymond MR, Bourke MAM, Von Dreele RB, Clausen B, Lorentzen T (1997) Use of Rietveld refinement for residual stress measurements and the evaluation of macroscale plastic strain from diffraction spectra. J Appl Phys 82:1554-1562

Daymond MR, Fitzpatrick ME (2006) Effect of cyclic plasticity on internal stresses in a Metal Matrix Composite. Metall Mater Trans A 37A:1977-1986

Daymond MR, Hartig C, Mecking H (2005) Interphase and intergranular strains in a composite with both phases undergoing plastic deformation. Acta Mater 53:2805-2813

Daymond MR, Lund C, Bourke MAM, Dunand DC (1999b) Elastic phase-strain distribution in a particulates reinforced Metal-Matrix Composite deforming by slip or creep. Metall Mater Trans 30A:2989-2997

Daymond MR, Priesmeyer HG (2002) Elastoplastic deformation of ferritic steel and cementite studied by neutron diffraction and self-consistent modelling. Acta Mater 50:1613-1626

Daymond MR, Tomé CN, Bourke MAM (2000) Measured and predicted intergranular strains in textured austenitic steel. Acta Mater 48:553-564
Daymond MR, Withers PJ (1996a) A new stroboscopic neutron diffraction method for monitoring materials subjected to cyclic loads: thermal cycling of metal matrix xomposites. Scripta Mater 35(6):717-720
Daymond MR, Withers PJ (1996b) A synchrotron radiation study of transient internal strain changes during the early stages of thermal cycling of MMCs. Scripta Mater 35(10):1229-1234
Dieter GE (1986) Mechanical Metallurgy. McGraw-Hill
Dobson D, Mecklenburgh J, Alfe D, Wood I, Daymond MR (2005) A new belt-type apparatus for neutron-based rheological measurements at gigapascal pressures. High Press Res 25:107-118
Dunst D, Mecking H (1996) Analysis of experimental and theoretical rolling textures of two phase titanium alloys. Z Metallkd 87:498-507
Dye D, Stone HJ, Reed RC (2001) A two phase elastic-plastic self-consistent model for the accumulation of microstrains in Waspalloy. Acta Mater 49:1271-1283
Edwards L, Bouchard PJ, Dutta M, Wang DQ, Santisteban JR, Hiller S, Fitzpatrick ME (2005) Direct measurement of the residual stresses near a "boat-shaped" repair in a 20 mm thick stainless steel tube butt weld. Int J Press Vessels Piping 82:288-298
Eshelby JD (1957) The determination of the elastic field of an ellipsoidal inclusion, and related problems. Proc Roy Soc A241:376-396
Eshelby JD (1959) The elastic field outside an ellipsoidal inclusion. Proc Roy Soc London Ser A 252:561-569
Fitzpatrick ME, Hutchings MT, Withers PJ (1997) Separation of macroscopic, elastic mismatch and thermal-expansion misfit stresses in Metal-Matrix Composite quenched plates from neutron-diffraction measurements. Acta Mater 45:4867-4876
Fitzpatrick ME, Lodini A (2003) Analysis of Residual Stress by Diffraction using Neutron and Synchrotron Diffraction. Taylor and Francis
Fitzpatrick ME, Withers PJ, Baczmanski A, Hutchings MT, Levy R, Ceretti M, Lodini A (2002) Changes in the misfit stress in an Al/SiC_p metal matrix composite under plastic strain. Acta Mater 50:1031-1040
Fonseca JQd, Bate PS, Oliver EC, Daymond MR, Withers PJ (2006) Modelling and measuring intergranular stresses during the early stages of plasticity. Acta Mater, submitted
Frischbutter A, Neov D, Scheffzuk C, Vrana M, Walther K (2000) Lattice strain measurements on sandstones under load using neutron diffraction. J Struct Geol 22:1587-1600
Gharghouri MA, Weatherly GC, Embury JD, Root J (1999) Study of the mechanical properties of Mg-7.7at% Al by *in situ* neutron diffraction. Philos Mag A 79:1671-1695
Gnaeupel-Herold T, Brand PC, Prask HJ (1998) Calculation of single-crystal elastic constants for cubic crystal symmetry from powder diffraction data. J Appl Cryst 31:929-935
Greenough GB (1947) Residual lattice strains in plastically deformed metals. Nature 160:258-260
Greenough GB (1952) Quantitative X-ray diffraction observations on strained metal aggregates. Prog Metal Phys 3:176-219
Gubicza J, Nam NH, Balogh L, Hellmig RJ, Stolyarov VV, Estrin Y, Ungar T (2004) Microstructure of severely deformed metals determined by X-ray peak profile analysis. J Alloys Compd 378:248-252
Hashin Z, Shtrikman S (1962) A variational approach to the theory of the elastic behaviour of polycrystals. J Mech Phys Sol 10:343-352
Hashin Z, Shtrikman S (1963) A variational approach to the theory of the elastic behaviour of multiphase materials. J Mech Phys Sol 11:127-140
Hauk V (1997) Structural and Residual Stress Analysis by Nondestructive Methods. Elsevier
Hill R (1952) The elastic behaviour of a crystalline aggregate. Prof Phys Soc London A 65:349-354
Hill R (1965) Continuum micro-mechanics of elastoplastic polycrystals. J Mech Phys Sol 13:89-101
Hosford WF (1993) The Mechanics of Crystals and Textured Polycrystals. Oxford
Howard CJ, Kisi EH (1999) Measurement of single crystal elastic constants by neutron diffraction from polycrystals. J Appl Cryst 32:624-633
Hutchings MT (1990) Neutron diffraction measurement of residual stress fields - the answer to the engineers' prayer? Nondestr Test Eval 5:395-413
Hutchings MT, Withers PJ, Holden TM, Lorentzen T (2005) Introduction to the Characterization of Residual Stress by Neutron Diffraction. Taylor and Francis
Hutchinson JW (1970) Elastic-plastic behaviour of polycrystalline metals and composites. Proc R Soc London A 319:247-272
Ikeda S, Carpenter JM (1985) Wide-energy-range, high-resolution measurements of neutron pulse shapes of polyethylene moderators. Nucl Instrum Methods Phys Res A239:536-544
Johnson MW, Daymond MR (2002) An optimum design for a time-of-flight neutron diffractometer for measuring engineering stresses. J Appl Cryst 35(1):49-57

Kamminga JD, Keijser THd, Mittemeijer EJ, Delhez R (2000) New methods for diffraction stress measurement: a critical evaluation of new and existing methods. J Appl Cryst 33:1059-1066
Kaschner GC, Tomé CN, Beyerlein IJ, Vogel SC, Brown DW, McCabe RJ (2006) Role of twinning in the hardening response of zirconium during temperature reloads. Acta Mater 54(11):2887-2896
Kocks UF, Mecking H (2003) Physics and phenomenology of strain hardening: the FCC case. Progr Mater Sci 48:171-173
Kocks UF, Tomé CN, Wenk H-R (1998) Texture and Anisotropy. Cambridge
Korsunsky AM, Daymond MR, James KE (2002) The correlation between plastic strain and anisotropy strain in aluminium alloy polcrystals. Mater Sci Eng A 334:41-48
Korsunsky AM, James KE, Daymond MR (2004) Intergranular stresses in polycrystalline fatigue: diffraction measurement and self-consistent modelling. Eng Fracture Mechanics 71 (4-6):805-812
Krawitz AD (2001) Introduction to Diffraction in Materials Science and Engineering. John Wiley and Sons
Krawitz AD, Winholtz RA (1994) Use of position-dependent stress-free standards for diffraction stress measurements. Mater Sci Eng A 185(1-2):123-130
Kröner E (1958) Zur Behandlung des Quantenmechanischen Vielteilchenproblems mit Hilfe von Mehrteilchenfunktionen. Z Physik 151:504-518
Kröner E (1961) Zur Plastischen Verformung des Vielkristalls. Acta Metall 9:155-161
Larsson C, Clausen B, Holden TM, Bourke MAM (2004) Measurements and predictions of strain pole figures for uniaxially compressed stainless steel. Scripta Mater 51:571-575
Levin VM, Alvarea-Tostado JM (2003) Eshelby's formula for an ellipsoidal elastic inclusion in anisotropic poroelasticity and thermoelasticity. Int J Fracture 119:4-2:L79-L82
Levy A, Papazian JM (1990) Tensile properties of short fibre-reinforced SiC/Al composites, part II. Finite element analysis. Metall Trans 21A:411-420
Lorentzten T, Daymond MR, Clausen B, Tomé CN (2002) Lattice strain evolution during cyclic loading of stainless steel. Acta Mater 50(6):1627-1638
Ma S, Brown D, Bourke MAM, Daymond MR, Majumdar BS (2005) Microstrain evolution during creep of a high volume fraction superalloy. Mater Sci Eng A 399:141-153
MacEwen SR, Faber J, Turner APL (1983) The use of time-of-flight neutron diffraction to study grain interaction stresses. Acta Metall 31:657-676
Martins RV, Margulies L, Schmidt S, Poulsen HF, Leffers T (2004) Simultaneous measurement of the strain tensor of 10 individual grains embedded in an Al tensile sample. Mater Sci Eng A 387:84-88
Matthies S, Priesmeyer HG, Daymond MR (2001) On the diffractive determination of elastic single crystal constants using polycrystalline samples. J Appl Cryst 34:585-601
Meredith PG, Knight KS, Boon SA, Wood IG (2001) The microscopic origin of thermal cracking in rocks: an investigation by simultaneous time-of-flight neutron diffraction and acoustic emission monitoring. Geophys Res Lett 28:2105-2108
Meredith PG, Wood IG, Knight KS, Boon SA (1997) *In situ* measurement of strain partitioning during rock deformation by neutron diffraction imaging. J Conf Abstracts 2:50
Mittemeijer EJ, Scardi P (2004) Diffraction Analysis of the Microstructure of Materials. Springer
Mura T (1987) Micromechanics of Defects in Solids. Nijhoff
Noyan IC, Cohen JB (1987) Residual Stress - Measurement by Diffraction and Interpretation. Springer-Verlag
Nye JF (1992) Physical Properties of Crystals. OUP
Oliver EC, Daymond MR, Withers PJ (2004a) Interphase and intergranular stress generation in carbon steels. Acta Mater 52:1937-1951
Oliver EC, Daymond MR, Withers PJ (2004b) Neutron diffraction study of extruded magnesium during cycling and elevated temperature loading. Materials Sci Forum 490-491:257-262
Oliver EC, Daymond MR, Withers PJ (2005) Effects of texture and anisotropy on intergranular stress development in zirconium. Mater Sci Forum 495-497:1553-1558
Oliver EC, Mori T, Daymond MR, Withers PJ (2003) Neutron diffraction study of stress induced martensite transformation and variant change in FePd. Acta Mater 51:6453-6464
Oliver EC, Mori T, Daymond MR, Withers PJ (2004c) Stress-induced martensitic transformation and variant change in an Fe-Pd shape memory alloy. Mater Sci Eng A 378:328-332
Oliver EC, Withers PJ, Daymond MR, Ueta S, Mori T (2002) Neutron diffraction study of stress induced martensitic transformation in TRIP steel. Appl Physics A 74:1143-1145
Pang JWL, Holden TM, Mason TE (1997) *In situ* generation of intergranular strains in Zircaloy under uniaxial loading. Acta Mater 47(2):373-383
Pang JWL, Holden TM, Mason TE (1998a) The development of intergranular strains in a high-strength steel. J Strain Analysis 33:373-383
Pang JWL, Holden TM, Mason TE (1998b) *In situ* generation of intergranular strains in an Al7050 alloy. Acta Mater 46:1503-1518

Parise JB (2006) High pressure studies. Rev Mineral Geochem 63:205-231
Pintschovius L, Prem M, Frischbutter A (2000) High precision neutron diffracion measurements for the determination of low level residual stresses in a sandstone. J Struct Geol 22(11-12):1581-1585
Poulsen HF, Wert JA, Neufeind J, Honkimaki V, Daymond MR (2005) Measuring strain distributions in amorphous materials. Nature Mater 1:33-36
Preuss M, Pang JWL, Withers PJ, Baxter GJ (2002) Inertia welding nickel-based superalloy: Part II. Residual stress characterization. Metall Mater Trans A 33:3227-3234
Pyzalla A, Camin B, Buslaps T, Di Michiel M, Kaminski H, Kottar A, Pernack A, Reimers W (2006) Simultaneous tomography and diffraction analysis of creep damage. Science 308 (5718):92-95
Raabe D, Zhao Z, Park SJ, Roters F (2002) Theory of orientation gradients in plastically strained crystals. Acta Mater 50:421-440
Redfern SAT (2006) Neutron powder diffraction studies of order-disorder phase transitions and kinetics. Rev Mineral Geochem 63:145-170
Reuss A (1929) Berechung der Fließgrenze von Mischkristallen auf Grund der Plastizitätsbedingung für Einkristalle. Z angew Math Mech 9:49-58
Rietveld HM (1969) A profile refinement method for nuclear and magnetic structures. J Appl Cryst 2:65-71
Rogan RC, Üstündag E, Clausen B, Daymond MR (2003) Texture and strain analysis of the ferroelastic behavior of Pb(Zr,Ti)O_3 by *in situ* neutron diffraction. J Appl Phys 93:4104
Ruud CO (1982) A review of selected non-destructive methods for residual stress measurement. NDT Int 15: 15-23
Sachs Z (1928) Zur Ableitung einer Fließbedingung. Z Ver Dtsch Ing 72:734
Sanitsteban JR, Oliver EC, Daymond MR, Alianelli L, Edwards L. (2006b) Tensile deformation of a Cu mosaic crystal along the <110> direction studied by time of flight neutron transmission. Mater Sci Eng A, in press
Santisteban JR, Daymond MR, Edwards L, James JA (2006a) ENGIN-X: a third generation neutron strain scanner. J Appl Cryst, in press
Santisteban JR, Edwards L, Fitzpatrick ME, Steuwer A, Withers PJ, Daymond MR, Johnson MW, Rhodes N, Schooneveld EM (2002) Strain imaging by Bragg edge neutron transmission. Nucl Instrum Methods A 481:765-768
Scheffzük C, Frischbutter A, Walther K (1998) Intracrystalline strain measurements with time-of-flight neutron diffractoin: application to a Cretaceous sandstone from the Elbezone (Germany). Schriftenreihe fur Geowissenschaften 6:39-48
Scheffzük C, Walther K, Frischbutter A, Eichhorn F, Daymond MR (2005) Residual strain and texture measurements using neutron TOF diffraction on a dolomite-anhydrite rock and a quartz-dunnite compound. Solid State Phen 105:61-66
Schofield PF, Covey-Crump SJ, Stretton IC, Daymond MR, Knight KS, Holloway RF (2003) Using neutron diffraction measurements to characterize the mechanical properties of polymineralic rocks. Mineral Mag 67:967-987
Schulson EM, Swainson IP, Holden TM (2001) Internal stress within hardened cement paste induced through thermal mismatch: Calcium hydroxide versus calcium silicate hydrate. Cement Concrete Res 31:1785-1791
Siano S, Bartoli L, Santisteban JR, Kockelman W, Daymond MR, Miccio M, Marinis Gd (2006) Non-destructive investigation of Picenum bronze artefacts using neutron diffraction. Archaeometry 48:77-96
Simmons G, Wang H (1971) Single Crystal Elastic Constants and Calculated Aggregate Properties: a Handbook. MIT Press
Šittner P, Lukáš P, Neov D, Daymond MR, Novák V, Swallowe GM (2002) Stress induced martensitic transformation in CuAlZnMn polycrystals investigated by two *in situ* neutron diffraction techniques. Mater Sci Eng A A324:225-234
Stone HJ, Holden TM, Reed RC (1999) On the generation of microstrains during the plastic deformation of Waspalloy. Acta Mater 47:4435-4448
Sun YN, Choo H, Liaw PK, Lu YL, Brown DW, Bourke MAM (2005) Neutron diffraction studies on lattice strain evolution around a crack-tip during tensile loading and unloading cycles. Scripta Mater 53(8): 971-975
Taylor GI (1938) Plastic strain in metals. J Instrum Methods 62:307-324
Tomé CN (1999) Self-consistent polycrystal models: A directional compliance criterion to describe grain interactions. Modell Simul Mater Sci Eng 7:723-738
Tomé CN, Maudlin PJ, Lebensohn RA, Kaschner GC (2001) Mechanical response of zirconium - I. Derivation of a polycrystal constitutive law and finite element analysis. Acta Mater 49:3085-3096
Turner PA, Christodoulou N, Tomé CN (1995) Modelling of the mechanical response of rolled Zircaloy-2. Int J Plasticity 11:251-265

Turner PA, Tomé CN (1994) A study of residual stresses in Zircaloy-2 with rod texture. Acta Mater 42:4143-4153

Üstündag E, Subramanian R, Dieckmann E, Sass SL (1995) In situ formation of metal-ceramic microstructures in the Ni-Al-O system by partial reduction reactions. Acta Metall Mater 43:383-389

Vaidyanathan R, Bourke MAM, Dunand DC (1999) Phase fraction, texture and strain evolution in superelastic NiTi and NiTi-TiC composites investigated by neutron diffraction. Acta Mater 47:3353-3366

Vogel SC, Priesmeyer H-G (2006) Neutron production, neutron facilities and neutron instrumentation. Rev Mineral Geochem 63:27-57

Voigt W (1910) Lehrbruch der Krystallphysik. Teubner

Von Dreele RB (2006) Neutron Rietveld refinement. Rev Mineral Geochem 63:81-98

Wang YD, Wang X-L, Stoica AD, Richardson JW, Peng RL (2003) Determination of the stress orientation distribution function using pulsed neutron sources. J Appl Cryst 36:14-22

Warren BE (1990) X-Ray Diffraction. Dover Publications

Watt JP (1980) Hashin-Shtrikman bounds on the effective elastic moduli of polycrystals with monoclinic symmetry. J Appl Phys 51(3):1520-1524

Watt JP, Peselnick L (1980) Clarification of the Hashin-Shtrikman bounds on the effective elastic moduli of polycrystals with hexagonal, trigonal, and tetragonal symmetries. J Appl Phys 51(3):1525-1531

Webster GA (2001) Polycrystalline Materials -- Determination of Residual Stresses by Neutron Diffraction. International Standards Organization, Report # TTA-3

Wenk H-R (2006) Neutron diffraction texture analysis. Rev Mineral Geochem 63:399-426

Wern H, Kock N, Maas T (2002) Selfconsistent calculation of the x-ray elastic constants of polycrystalline materials for arbitrary crystal symmetry. Mater Sci Forum 404:127-132

Wilkinson AJ (1997) Methods for determining elastic strains from electron backscatter diffraction and electron channelling patterns. Mater Sci Technol 13:79-84

Withers PJ (2004) Depth capabilities of neutron and synchrotron diffraction strain measurement instruments. I The maximum feasible path length. J Appl Crystall 37:596-606

Withers PJ, Clarke AP (1998) A neutron diffraction study of load partitioning in continuous Ti/SiC composites. Acta Mater 46:6585-6598

Withers PJ, Daymond MR, Johnson MW (2001) The accuracy of diffraction peak location. J Appl Cryst 34: 737-743

Withers PJ, Preuss M, Webster PJ, Hughes DJ, Korsunsky AM (2002) Residual strain measurement by synchrotron diffraction. Mater Sci Forum 404:1-10

Withers PJ, Stobbs WM, Pedersen OB (1989) The application of the Eshelby method of internal stress determination for short fibre metal matrix composites. Acta Metall Mater 37:3061-3084

Xu F, Holt RA, Daymond MR (2006) Development of internal strains during uni-axial deformation in textured Zircaloy-2: Part 2 modelling. Acta Mater, submitted